Marine Geology 460 (2023) 107051

Contents lists available at ScienceDirect

Marine Geology

journal homepage: www.elsevier.com/locate/margo

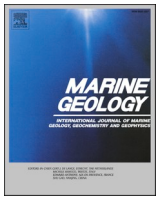

Temporally variable recurrence regimes of mega-tsunamis in the 6500 years prior to the 2004 Indian Ocean event

Jaishri Sanwal [a,*], C.P. Rajendran [a,b], Mohammad Heidarzadeh [c], Swapnil Mache [d,f], K. Anandasabari [e], Kusala Rajendran [f]

[a] Geodynamics Unit, Jawaharlal Nehru Centre for Advanced Scientific Research, Bengaluru 560064, India
[b] National Institute of Advanced Studies, Bengaluru 560012, India
[c] Department of Architecture and Civil Engineering, University of Bath, Bath BA2 7AY, United Kingdom
[d] Biomedical Photonic Imaging Group, University of Twente, 217, 7500 AE Enschede, Netherlands
[e] National Institute of Ocean Technology, Chennai 60010, India
[f] Centre for Excellence on Advanced Mechanics of Materials, Department of Civil Engineering, Indian Institute of Science, Bengaluru 560012, India

ARTICLE INFO

Keywords:
Indian Ocean
The 2004 earthquake
Subduction zone
Tsunami recurrence
Supercycles

ABSTRACT

The analyses of cores retrieved from three sites near Port Blair (South Andaman) revealed out-of-sequence deposits at various depths. They are identified as previous episodes of tsunami by their sediment characteristics and microfossil content, using the 2004 event deposition as a template. These deposits have median ages of 601 cal. yr BP, 837 cal. yr BP, 1440 cal. yr BP, 3018 cal. yr BP, 3591 cal. yr BP, 4712 cal. yr BP, 5607 cal. yr BP, and 6357 cal. yr BP and are chronologically equivalent of those from the far-field locations in the Indian Ocean region. The distant deposits that are correlated with the South Andaman sites most likely owe their origin to the 2004-type events, as indicated by tsunami simulations in the study region. The long-term record presented here is characterized by an early phase of a quasiperiodic recurrence regime that transitions into a distinct interval of temporally clustered events. The quasiperiodic regime that appears around the mid-Holocene with an inter-event interval of 980 ± 385 years is followed by a sizable quiescent period of 1605 ± 245 years, before being succeeded by a regime of temporally clustered events. The chronology of nine tsunami events in the last 6500 years from the Indian Ocean region, thus implies a nonlinear pattern for the causative earthquakes. As demonstrated in the subduction zones elsewhere, the temporal variability of tsunamigenic great earthquakes is supported by the theoretical models espousing the characteristics of long-term stress recycling processes active within the subduction zones and transfer processes between the lower viscoelastic layer and the upper seismogenic crust.

1. Introduction

Sourced from Banda Aceh, Sumatra Island, the M_w 9.1 earthquake of December 26, 2004, generated a massive tsunami in the Indian Ocean (Figs. 1A and B). The earthquake rupture propagated northward, terminating near the northern tip of the Andaman Islands chain, spanning 1200 km (Ammon et al., 2005). The ensuing tsunami impacted the shores of the littoral countries of the Indian Ocean, including the distant coast of East Africa. The transoceanic reach of the 2004 tsunami stands out in contrast to the limited reach of two hypothetical tsunamis from this region triggered by lesser magnitude earthquakes, as shown in Figs. 2A-C (for details, see later discussion). The 2004 tsunami was a highly unusual event in terms of its magnitude and the extensive transoceanic effects it produced. As a result, there is much scientific interest in investigating whether such mega tsunamis had occurred in the past and how frequently they may have occurred. However, due to the infrequency of such occurrences in this area prior to the 2004 tsunami, there has been limited research conducted on this topic in the past. The post-2004 studies conducted in various parts of the Indian Ocean region have focused on examining sedimentation records in coastal depositional environments to establish a chronological framework to gain insight into the occurrence and frequency of past tsunamis (see Fig. 1A for specific study locations). Identification of tsunami deposits is often based on recognizing anomalous sand sheets in low-energy environments such as coastal ponds, lakes, and marshes, which trap microfossil assemblages of neritic and open ocean affinity (Goff

* Corresponding author.
E-mail address: jaishrigeology@gmail.com (J. Sanwal).

https://doi.org/10.1016/j.margeo.2023.107051
Received 14 November 2022; Received in revised form 6 April 2023; Accepted 17 April 2023
Available online 22 April 2023

et al., 2012; Andrade et al., 2014; Costa et al., 2021; Satake et al., 2020). Tectonic constraints based on estimating land-level changes evident from the subsided mangrove swamps and uplifted coral terraces in the near-field areas have also been used to supplement the tsunami studies (Rajendran et al., 2007; Malik et al., 2011; Rajendran, 2013). Such evidentiary information has been useful in developing the tsunami-earthquake recurrence models in the Indian Ocean.

During the initial phase of the post-2004 tsunami studies, a paleo-tsunami between 1250 and 1450 CE was reported from Thailand and Sumatra (Jankaew et al., 2008; Monecke et al., 2008). This event is also chronologically equivalent to an episode of well-dated coral uplift located off Sumatra (Meltzner et al., 2010). Yet another older tsunami of 770–1040 CE was construed from Sumatra by Monecke et al. (2008), whose footprints were found also along the Andaman and Nicobar (A&N) Islands and the southeastern coast of India (Rajendran et al., 2007, 2011, 2013). Further, sediment cores from distant coastal lagoons located in Sri Lanka and the Maldives had revealed much older tsunamis (Jackson et al., 2014; Klostermann et al., 2014). A timeline of eleven tsunamis between 2900 and 7400 years was identified from a stack of alternating layers of transported debris from a coastal cave in Aceh, Sumatra, close to the epicentral area (Rubin et al., 2017). Using turbidite deposits, off Sumatra, from the southern part of the 2004 source zone, Patton et al. (2015) reported a 6600-year-long record of earthquakes. As the region hosts several independent seismic sources, it is likely that the turbidite sequence may hold the chronological clues of the locally sourced earthquakes as well as those originating from the 2004 rupture zone.

This caveat becomes apparent in a recent study of tsunami deposits from the South Andaman, from where Malik et al. (2019) recorded six tsunami deposits. While the younger ones, in this study, are attributed to the local lesser magnitude earthquakes of 1881 (M_w 7.9; source: Car Nicobar), 1762 ($M_w \leq 8.5$; source: Arakan Coast, Myanmar), 1679 (unknown magnitude; likely source: North Andaman); the older tsunamis fall in the age brackets of650–550 yr. BP (1300–1400 CE), 3950–4950 yr. BP (2000–3000 BCE), and 4760–5150 yr. BP (2810–3200 BCE)- with unspecified sources and sizes of the respective events (Fig. 3A). Considering the uncertainties of sizes of the previous earthquakes and the reach of the consequent tsunamis in the region, our present work is thus designed to develop an independent authentication of the long-term record of the 2004-type transoceanic tsunamis that could have originated from repeated breaks on the full breadth of the Andaman-Sumatra subduction zone interface, and how the earthquake cycle operating here agrees with the available models of earthquake recurrence.

For forecasting large earthquakes, an important input to be considered is the past record of large earthquakes that informs if they recur regularly, randomly, or cluster together in time (Griffin et al., 2020). Elastic rebound theory, the dominant paradigm in seismology, predicts that large earthquakes recur in regular intervals following the cycle of periodic accumulation of strain and its release (Reid, 1910). The numerical models and simulations, however, offer multiple choice of recurrence patterns that can be termed as strongly periodic, weakly periodic, Poissonian or bursty (Salditch et al., 2020). The validation of these models should come from the geological studies of the fault zones. Many times, the paleoseismic records are not long enough to offer the actual picture of spatio-temporal patterns of earthquake occurrences, although a few available geological records do indicate complex patterns of earthquake recurrence patterns including clustering along the subduction zone located west of Sumatra, Indonesia, and the Cascadia region in the northwest America (e.g., Sieh et al., 2008; Salditch et al., 2020; Philibosian and Meltzner, 2020), contrary to what is predicted in elastic rebound theory.

We report here independently derived stratigraphic data from a few sites in South Andaman to develop a near-field long-term template of tsunami deposition to identify chronologically comparable tsunami litho-units available from other parts of the Indian Ocean littoral impacted by the 2004 tsunami. Our present work is designed to develop an authentication of the long-term record (~6500 years) of 2004-type

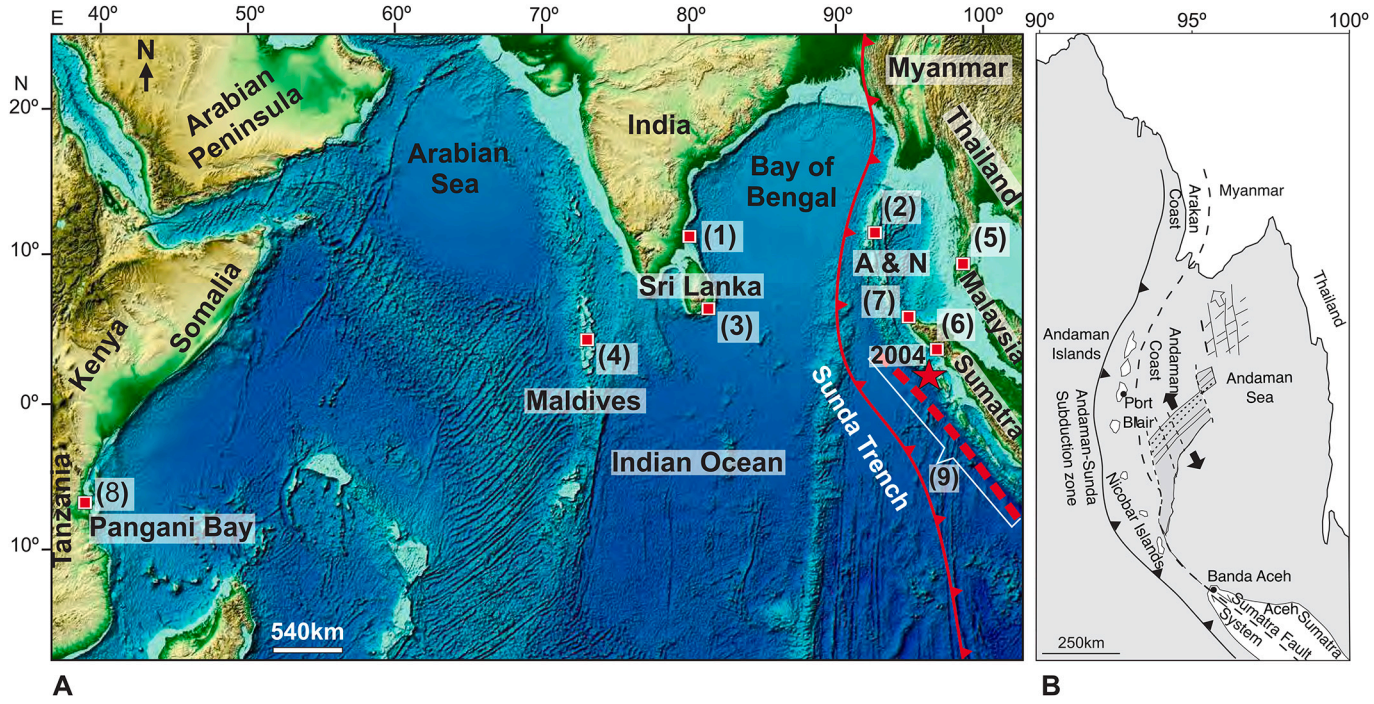

Fig. 1. A. Map showing the Indian Ocean region and the source region of the 2004 (Mw 9.2) earthquake, marked by red filled pentagram; A&N: Andaman Nicobar Islands, MA: Maldives and SL: Sri Lanka. Paleotsunami sites are marked by red filled squares: 1. (Rajendran et al., 2006, 2011); 2. (Rajendran et al., 2013); 3. (Jackson et al., 2014); 4. (Klostermann et al., 2014); 5. (Jankaew et al., 2008); 6. (Monecke et al., 2008); 7. (Rubin et al., 2017); 8. (Sieh et al., 2014; Maselli et al., 2020). 9. A few deep-sea sediment core sites are marked by the dotted red lines (Patton et al., 2015); **B.** Map of the area showing the subduction zone and various tectonic units of the A&N region

transoceanic tsunamis. This database is useful not only to evaluate the long-term behavior of a major tsunamigenic source (Fig. 1) but also helpful in developing realistic forecast models of mega-earthquakes in the region.

2. Material and methods

The Andaman and Nicobar group of islands, between the Bay of Bengal in the west and the Andaman Sea in the east, form a part of the outer arc ridge of the northern segment of the Sunda subduction zone (Fig. 1B). These islands have witnessed coseismic subsidence as well as uplift during the 2004 earthquake. The subsided coastal tracts along these islands have proven to be ideal repositories of tsunami deposits. The area of the present study is the South Andaman Coast, located within a region that subsided by ~1 m during the 2004 earthquake (Rajendran et al., 2008; Fig. 3A). Waves travelled nearly 1 km inland and deposited thick sheets of sediments in the marshes. To compare the alternate scenarios of tsunamis directivity and consequent near and distant coastal impacts, simulations were conducted for two hypothetical M_w 8.5 earthquakes based on their sources within the Sumatra-Andaman region, in addition to the 2004 event. This helps in benchmarking the far-field propagation pattern of lesser magnitude tsunamis with assumed rupture geometries as compared to the 2004 event. This exercise would help in inferring the transoceanic reach of such tsunamis

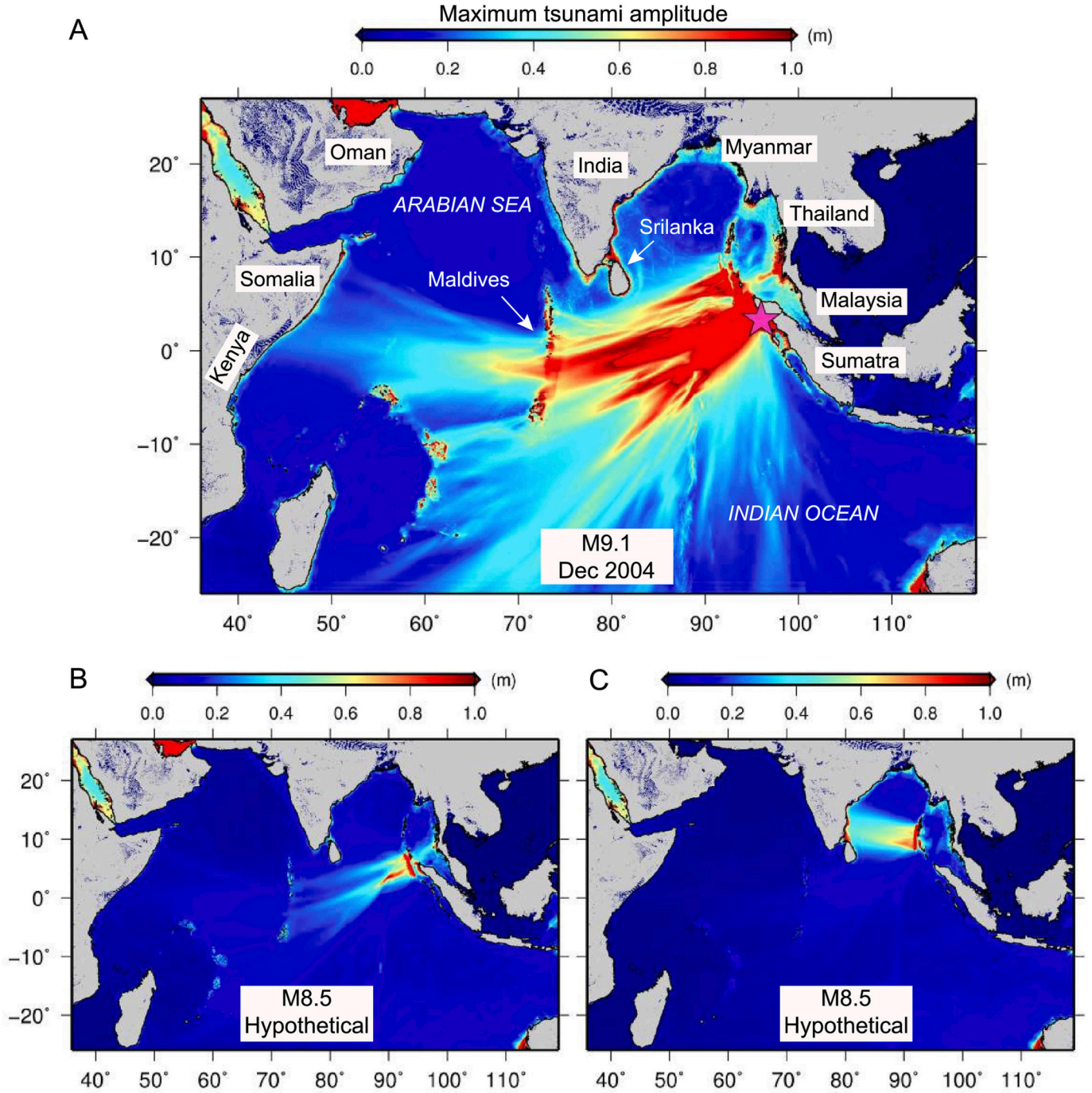

Fig. 2. Results from tsunami modeling. **A.** The M_w 9.1 December 2004 earthquake; **B and C.** Two hypothetical M_w 8.5 events sourced from two hypothetical source regions within the Sumatra-Andaman subduction zone. The results represented in A, B, and C correspond to crustal deformations shown in Figs. 10A, B, and C, respectively.

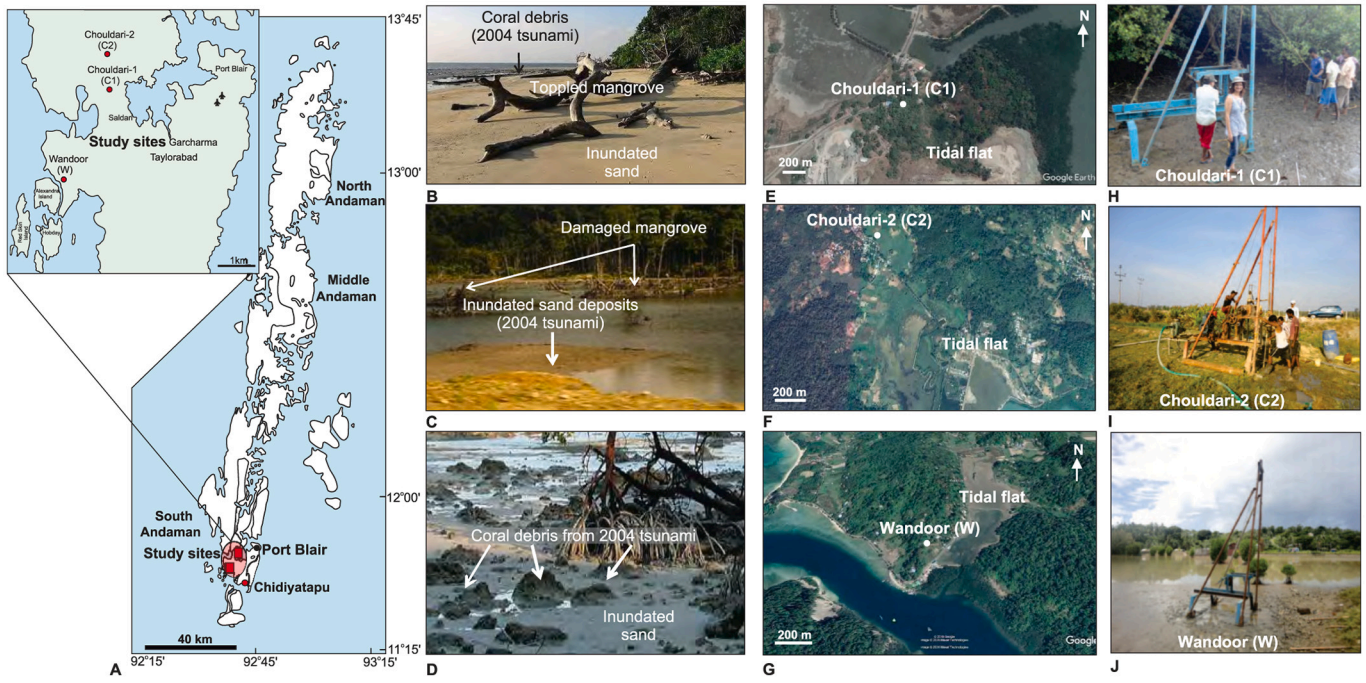

Fig. 3. A. Map of Andaman Island and study area (red-filled squares inside the Highlighted circle), inset shows the locations of the present study sites in south Andaman and an earlier sampling site (red-filled circle) by Malik et al. (2019). **B—C.** Photographs of coral debris, inundated sand, and toppled mangrove deposited during the 2004 tsunami near Chouldari-1 (C1) and Chouldari-2 (C2) sites. **D.** Close-up views of coral boulders and sand were deposited during the 2004 tsunami near Wandoor (W) site. ***E*-G.** Close-up views of the coring sites: C1, C2, and W, near Port Blair South Andaman. H-J. Field photographs of coring at C1, C2, and W sites, using a weighted tripod system. (For interpretation of the references to colour in this figure legend, the reader is referred to the web version of this article.)

and understand if such hypothetical lesser magnitude events would overlap the far-field inundation spatial coverage of the 2004 event, including the study sites used in this study.

As one explores high-energy coastal depositional settings, there is always the challenge of discriminating between the tsunami and storm deposits (Morton et al., 2007). Substantial efforts have been made to characterize the 2004 tsunami deposits and their stratigraphic and sedimentary properties, both along the southeast coast of India and the Andaman Islands (Nagendra et al., 2005; Srinivasalu et al., 2007; Rajendran et al., 2007; Srinivasalu et al., 2009). These observations document features like multiple upward fining sequences characterized by deposits of broken shells, coral fragments, and coarse carbonate gravel with significant variation in the sediment thickness and composition.

In the present case, we rule out the possibility of storm surges as a potential depositional mechanism in our study sites, because of the near absence of high inundation impact from the cyclones, though the neighboring oceanic region is most vulnerable to the development of low-pressure zones and cyclonic storms (India Meteorological Department, 2008). The historical storm records indicate the cyclonic impact on the Andaman Islands in 1911, 1914, 1916, 1921, 1961, 1976, and 1989. The storms caused only minimal coastal surges as determined by the wind speed and precipitation intensity (Satish Kumar et al., 2008). Previous studies have utilized historical records, simulations, and geospatial techniques to investigate the long-term impact of severe cyclonic events in the Andaman Islands. These studies suggest that the region is less vulnerable to cyclone surges (Satish Kumar et al., 2008; Varikkodan et al., 2023). According to the simulations conducted by Satish Kumar et al. (2008), even under a super-cyclone with a maximum wind speed of 80 m/s, the surges on the coastal areas of the islands are only expected to reach <4.0 m above mean sea level. Our study sites in South Andaman are situated far inland, away from the impact of such storm surges (see Fig. S1).

Although both storm and tsunami deposits can be caused by similar mechanisms, they can be differentiated based on their sedimentary and stratigraphic characteristics. We have conducted the detailed characterization of the alternate bands of coarser sediment referred to as 'out-of-sequence' or allochthonous/event layers within the dominantly marshy/tidal depositional regime. Several previous studies on the characterization of the tsunami deposits, such as poor sorting of the sediments (Cordova, 2014) and bimodal grain size distribution of sand (Moore et al., 2007). Unlike storm deposits, which tend to be well-sorted and composed of a narrower range of grain sizes, tsunami deposits exhibit a wide range of grain sizes, including large-sized clasts (Moore et al., 2007; Sawai et al., 2012). The stratigraphic context of the tsunami deposits includes sharp boundaries with the in-situ sediments, which helps to distinguish them from storm deposits that form more gradual boundaries (Sawai et al., 2012). As reported in some previous studies, tsunami deposits may contain sedimentary structures, including rip-up clasts and mud drapes, which are generally absent in storm deposits because of the intense turbulence and prolonged agitation of storm waves, which leads to the fragmentation and dispersion of clasts (Dawson, 1994; Goff et al., 2001; Jaffe et al., 2008). It has been noted that the lithological characteristics of tsunami deposits and their spatial dispositions are influenced by the composition of the shelf sediment and the coastal topography (Gelfenbaum et al., 2007; Hori et al., 2007). Thus, collectively, most of the previous studies conclude that the local morphology, the velocity of tsunami waves, and the source/depositional environment greatly affect the tsunami deposit characteristics. Overall, these studies provide valuable insights into the effects of local morphology, tsunami wave velocity, and source/depositional environment on the characteristics of tsunami deposits, which can aid in site selection, stratigraphic interpretation, and identification of past tsunami deposits.

The near-field results presented in this study are derived from a few coring sites near the capital town of Port Blair, South Andaman. Being close to the sea and heavily impacted by the 2004 tsunami, the area identified for coring offered an ideal depositional environment with a

fair degree of preservation potential. The depositional environment appears conducive for the preservation of deposits left by repeated previous high-energy sea inundations likely to have affected this region.

Three sites, namely, Chouldari-1 (C1), Chouldari-2 (C2), and Wandoor (W), were selected for coring (Fig. 3A and E-G), at an elevation of ~25 ft. (7.6 m) (C1), ~20 ft. (6 m) (C2), and ~ 18 ft. (5.5 m) (W), respectively (see. Fig. S1 for the topographic profile of the study area and locations of cores). All the coring sites mentioned here are located within or near the narrow bays impacted by the 2004 tsunami. As reported in Dharanirajan et al. (2007), the maximum inland limit reached by the 2004 tsunami was 1320 m in the Wandoor settlement area. As demonstrated during the 2004 tsunami, these narrow bays offered focused pathways for inundation and facilitated the propagation of wave's further inland. Among the coring sites, the topmost sedimentary zone at Chouldari-2 was much disturbed due to the agricultural activities, and therefore we have discarded ~1-m-thick top-sediment cover to avoid any contamination. It is important to note that the coring site (W) at Wandoor is situated closer to the tidal inlets as compared to Chouldari-1 and, therefore, experiences relatively a greater tidal impact. This could be a reason some of the older depositional events are absent in Wandoor, as they may have been eroded away by the tidal currents in the area.

The percussion drilling was employed using a weighted tripod system with 1.5-m-long plastic liners. The total recovery of sediment cores at these three sites was 4.1 m (C1), 3.4 m (C2), and 8.6 m (W) (see Figs. 3H-J) without losing any amount of sediment. Our initial examination of the cores from all three drill sites helped demarcate alternating lighter-colored layers of coarser materials within dark-colored fine-grained sediments as they appeared in the computed tomography scan images (Figs. S2A—C). We have relied on the lithology, grain size analysis, and assemblage characteristics of foraminifera, in addition to the presence of plant and shell debris to characterize the stratigraphic units. The lithology retrieved from the cores comprises homogeneous dark-colored peat and peaty silt, signifying a low-energy marsh environment. These deposits are alternated with layers of coarser sediments (Figs. 4A-C; S1A—C). We define this disturbed sequence of coarser deposits as the 'event deposit/layer.' (See Fig. 5.A.)

The analyses of foraminifera from the cores were conducted from the homogeneous peaty sediment and intermittent event layers at intervals of 10 cm. After removing the organic matter, the samples were sieved with ASTM mesh sizes 60, 100, and 230. Foraminifera were picked using 60 and 100-mesh fractions. To reconstruct the timings of the event deposits, we have generated the radiocarbon dates of the organic-rich sediments. Buried organic-rich sediment from the top and bottom layers or within the allochthonous/event deposits were chosen for dating (Tables 1; S1). We have generated a total of twenty-five ^{14}C dates from the cores from sites: C1, C2, and W (Table S1). The dates are obtained from organic-rich and peat sediments. The ages of soil burial were calibrated using CALIB (version 7.0.2; Reimer et al., 2013). The calibrated age ranges are shown with two standard deviations, expressed as 'before present' (BP) and years CE and BCE with reference to 1950. The age data, in most cases, provided maximum and minimum ages of the inferred event deposits (Figs. 4A-C; S3). The final estimated ages of the events are captured within the time ranges spanning from the youngest possible (above the deposit) to the oldest possible (below the deposit). The possible ages of six depositional events (*E*-II, E-III, E-V, E-VI, E-VIII, and E-IX) are estimated by taking the average time range from the oldest to youngest (Fig. S4).

The age interval of another set of two ancient depositional events is calculated by taking the midpoint of the time range from a single age obtained from within the event layers (Fig. S4). Furthermore, the age data obtained from the top and the bottom of the event layers and from within show minimum error. In the present study, most of the age data is utilized for interpreting the chronology of the tsunamis (see Table 1). We have also recovered a few modern ages, marked in red, to provide constraints on Event-1 (E-1) (Fig. 4 and Table S1). The timings of the event depositions are reported in μ ±2σ ranges (μ = mean, σ = standard deviation) for our results as well as for those reported from elsewhere in the Indian Ocean region. We have identified nine layers of event depositions in the cores that are considered here as having been deposited by various tsunami events (Figs. 4A-C). The ages are rounded off to the decade, including the 2 σ range to describe the chronology of events and their comparison with other sites (see Table. 1 for ^{14}C age data and calibrated ages).

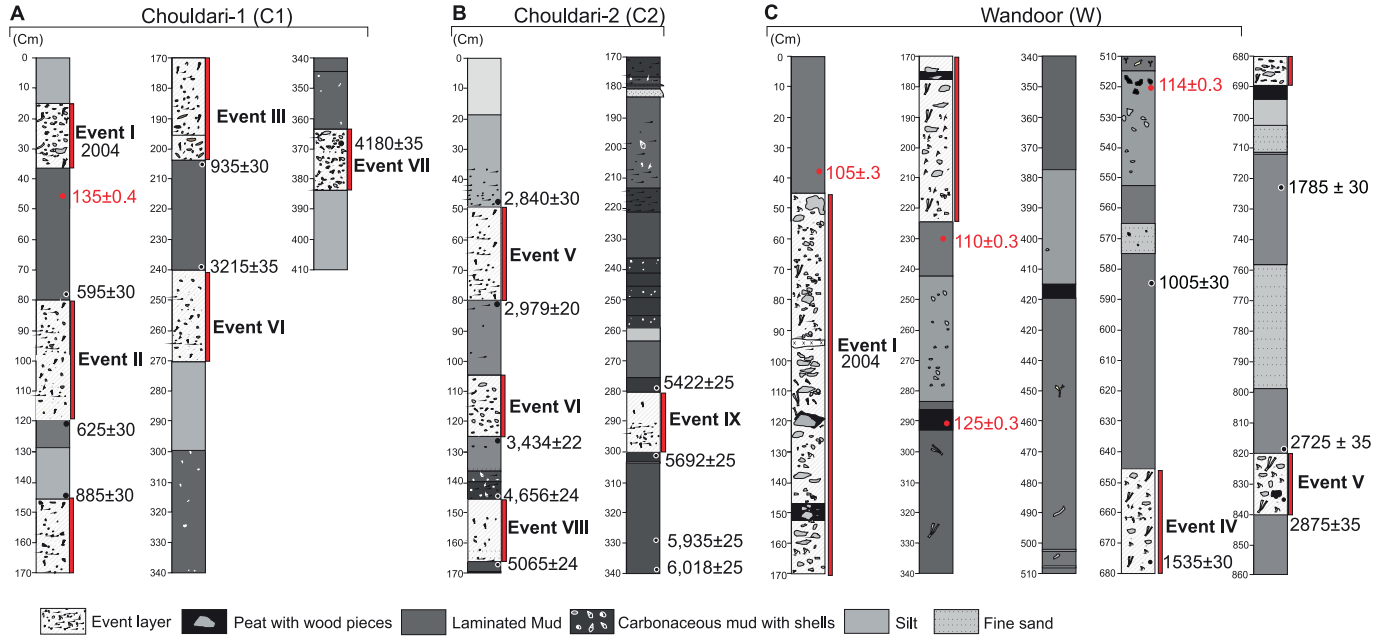

Fig. 4. Lithologs from the study sites: **A.** Chouldari-1 (C1), **B.** Chouldari-2 (C2), and **C.** Wandoor (W), near Port Blair, South Andaman. The locations of radiocarbon dating are marked with black-filled circles and the red-filled circles including numbers in red shows the modern ages and their locations. The event layers are marked with thick red lines. (For interpretation of the references to colour in this figure legend, the reader is referred to the web version of this article.)

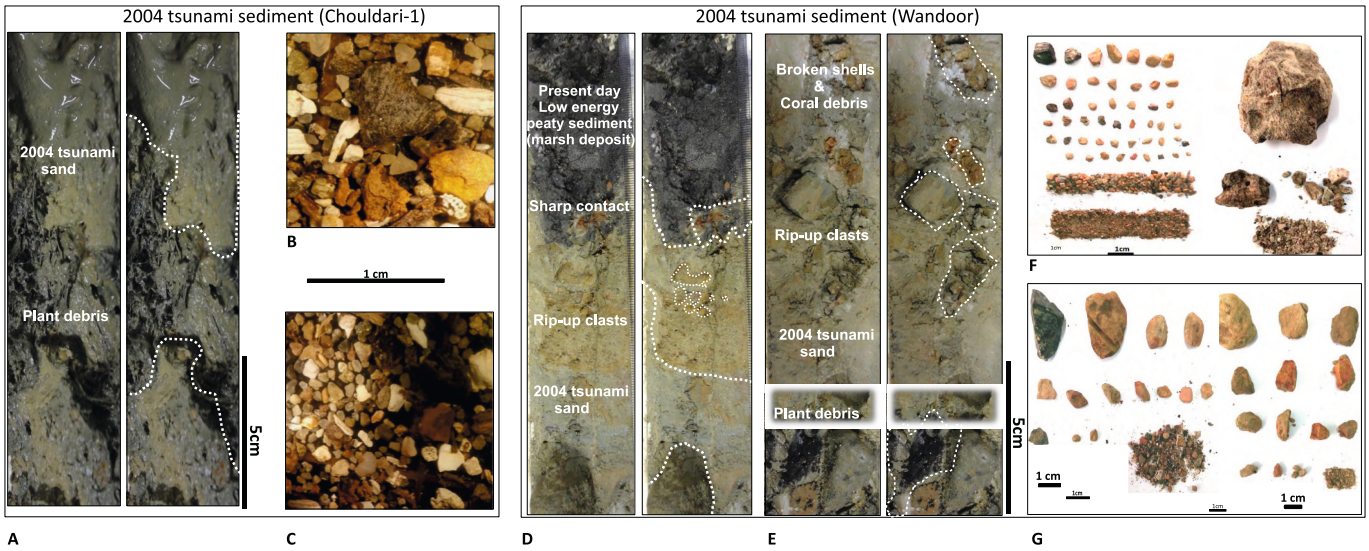

Fig. 5. A. Close-up views of the event deposit transported during the 2004 tsunami, recovered from the core collected at Chouldari-1; **B-C**. Microscopic view of the coarse-grained fraction of event deposit (2004 tsunami) from Chouldari-1 core; **D-E**. Close-up views of 2004 tsunami deposit, recovered from Wandoor core; **F-G**. Photographs show the coarse-grained fraction separated from the event sediment layers; transportation marks are often seen in the coarser clast. The particles shown here are part of the macro (>2 mm) fraction.

Table 1
Radiocarbon (AMS) ages of tsunami events, obtained using the charcoals from the organic-rich sediments. The analyses were conducted at Poznan Radiocarbon Laboratory (Poz), Poland. Radiocarbon ages were calibrated using CALIB (Version 7.0.4) (Stuiver and Reimer, 1993; Reimer et al., 2013). The 2 sigma ranges have maximum area under the probability distribution curve.

Event	Depth from surface (cm)	Thickness of the sediment (cm)	Age above tsunami deposit (μ ± 2σ calendar yr BP) (Calibrated ages (BCE/CE)	Age below tsunami deposit (μ ± 2σ calendar yr BP) (Calibrated ages (BCE/CE)	Age within the deposit (μ ± 2σ calendar yr BP) (Calibrated ages (BCE/CE)	Midpoint age of the tsunami deposits	Sites
Event 1 (E-I)	15	20		*Known Event (2004 CE)*			Chouldari-1
	45	180					Wandoor
Event 2 (E-II)	80	40	595 ± 30 (1298-1410 CE)	625 ± 30 (1290–1398 CE)		1349 CE	Chouldari-1
Event 3 (E-III)	147	60	885 ± 30 (1042–1219 CE)	935 ± 30 (1027–1161 CE)		1113 CE	Chouldari-1
Event 4 (E-IV)	645	45			1535 ± 30 (428–592 CE)	510 CE	Wandoor
Event 5 (E-V)	820	20	2725 ± 35 (967–808 BCE)		2875 ± 35 (1192–930 BCE)	1068 BCE	Wandoor
	835						
	50	30	2840 ± 30 (1107–917 BCE)	2979 ± 20 (1262–1127 BCE)			Chouldari-2
Event 6 (E-VI)	105	20		3434 ± 22 (1872–1666 BCE)		1641 BCE	Chouldari-2
	240	30	3215 ± 35 (1606–1417 BCE)				Chouldari-1
Event 7 (VII)	365	20			4180 ± 35 (2888–2635 BCE)	2762 BCE	Chouldari-1
Event 8 (E-VIII)	145	20	4656 ± 24 (3516–3366 BCE)	5065 ± 24 (3950–3797)		3657 BCE	Chouldari-2
Event 9 (E-IX)	280	20	5422 ± 25 (4336–4244 BCE)	5692 ± 25 (4586–4456 BCE)		4407 BCE	Chouldari-2

Note: AMS dating of charcoal samples were conducted at Poznan Radiocarbon Laboratory (Poz), Poland. Radiocarbon ages were calibrated using CALIB (Version 7.0.4) (Stuiver and Reimer, 1993; Reimer et al., 2013). The 2 sigma ranges have maximum area under the probability distribution curve. All samples are taken from organic-rich bulk sediment.

3. Results

3.1. Simulation study

We conducted tsunami simulations for two hypothetical M_w 8.5 events with different source regions and compared their impacts with the 2004 Indian Ocean tsunami (see Fig. 2 for tsunami simulations). It can be seen in Fig. 2A that the December 2004 tsunami significantly impacted the coastlines across the Indian Ocean, from near-field (Indonesia, Nicobar-Andaman, Thailand, Myanmar, and Malaysia) to far-field (southeast India, Sri Lanka, the Maldives, Seychelles, Mauritius, Madagascar, East Africa, and Oman). The hypothetical M_w 8.5 earthquake that generated a tsunami from the north of Sumatra (Fig. 2B) significantly impacted Sumatra and the parts of distant regions such as

Thailand, Myanmar, India, Sri Lanka, and the Maldives, with minor tsunami amplitudes also reaching the islands of Seychelles, and Mauritius, and the eastern coast of Africa. The hypothetical M_w 8.5 event from the Andaman Islands mostly affects Thailand, Myanmar, India, and Sri Lanka (Fig. 2C). The simulations were performed using the numerical package COMCOT (Cornell multigrid coupled tsunami model; Liu et al., 1998; Wang and Liu, 2006; Heidarzadeh et al., 2020, 2022). We applied linear tsunami simulations on a spherical grid system and used a single uniform grid with a spatial resolution of 2 arc-min. As our purpose was to study the far-field propagation pattern of tsunamis and as no inundation was included in our simulations, such a bathymetric grid was sufficient. Although inundation is not included in our modeling, the tsunami modeling of this study has proved to be helpful towards identifying the far-field depositional reach of large tsunamis, as shown by Satake et al. (2020). The bathymetry data is from the 2020 edition of the GEBCO (General Bathymetric Chart of the Oceans) global digital bathymetry atlas (Weatherall et al., 2015). A time step of 1.5 s was considered for the simulations. Co-seismic crustal deformations were calculated using the Okada (1985) dislocation model and were used as the initial conditions for the simulations. We considered three scenarios for large earthquakes and tsunamis: (i) The M_w 9.12004 Sumatra-Andaman earthquake based on the source model by Fujii and Satake (2007); (ii) A hypothetical M_w 8.5 earthquake to the north of Sumatra; and (iii) Another hypothetical M_w 8.5 event around the Andaman Islands (Figs. 2A-C). The M_w 9.1 model of Fujii and Satake (2007) is a heterogeneous model, while the two M_w 8.5 models involve uniform slips. For the M_w 8.5 events, we use the following fault parameters: length 500 km, width 100 km, slip 4 m (uniform), strike angle 335.0° and 0.0° for events (ii) and (iii), respectively, dip angle 10°, and rake angle 90°. Tsunami modeling in this study aims to understanding the far-field propagation patterns of tsunamis from megathrust earthquakes in the Sumatra-Andaman subduction zones. While our modeling effort informs about potential locations for tsunami deposition in the far-field and can give qualitative information about tsunami deposition, it is unable to provide details about the thickness of tsunami deposition and related particulars as such accuracy cannot be achieved given current computational and bathymetric/topographic limitations (e.g., Satake et al., 2020).

3.2. Age determination

Excluding the 2004 deposits (present at Wandoor and Chouldari-1), we have identified eight anomalous/event layers of coarser sediments in the cores that range in age from ~600 to 6500 years (Figs. 4A-C). The anomalous layers discovered at greater depths exhibit striking sedimentary resemblances to the deposits left behind by the 2004 tsunami. These layers can be distinguished from the ones formed by cyclones due to their distinct sedimentary structure, grain size, depositional and erosional contacts, which provide a clear differentiation between these anomalous layers and other storm deposits. These deposits comprise silica-rich mud dominated by quartz grains, coarse sand, and pebbles along with intact and fragmented shells, including plant and coral fragments (Figs. 5A-G; 6A-I). The sieve analyses of the sediment from the cores, following the size classifications of Folk and Ward (1957), were conducted with a resolution of 5–10 cm (Fig. 7). The large-size pebbles, broken shells, coral fragments, and organic debris in the sediment were removed with the help of forceps. The samples were dried in a hot air oven at about 50 °C and treated with HCL (30%) to eliminate the carbonate material. The organic matter was removed by treatment with H_2O_2.

The OxCal program (Bronk Ramsey, 2008) was used to model the recurrence pattern of the tsunami deposits. The radiocarbon ages of the eight anomalous layers and the 2004 tsunami event were included to model the inter-event periods, that is, the interval between events II and I, III and II, and so forth. Using the Difference() function in OxCal, we subtracted the ages of two consecutive deposits from each other to obtain a probability distribution of the corresponding inter-event period. The Difference() function in OxCal models the inter-event periods is similar to BACON (Blaauw and Christen, 2011), that is, by obtaining probabilistic descriptions of the periods by subtracting the ages of consecutive tsunami deposits within each Markov chain Monte Carlo iteration (Kempf et al., 2019). We repeated this analysis for all the events to get the overall interval distribution, represented by the OxCal ages in 2σ ranges that are rounded off to 5 years.

3.3. Identification of Tsunami deposits

The study region is marked by a chain of marshes and tidal channels, which lie within the tsunami reach, as revealed during the 2004 inundation patterns (Figs. 3B-D and Fig. S1). At all three sites, namely Chouldari-1 (C1), Chouldari-2 (C2), and Wandoor (W), the stratigraphy of the core sediments generally consists of in-situ marshy, low-energy dark-colored peat and peaty silt, with occasional layers of coarse-grained tsunami sediments. As compared to 'C2', which is located slightly far from the sea within the marshy environment, the other two marshy sites, 'C1' and 'W'; are situated close to the tidal inlets. The 2004 tsunami deposits recovered from two sites (C1 and W) but were not found in the 'C2' site, probably due to human intervention in recent years as it is close to the settlements. The 2004 tsunami deposits in both the sites (C1 and W) vary in thickness, ranging from 20 to 180 cm, and are mostly composed of poor to moderately sorted medium to very coarse sand. A Close view of the 2004 tsunami sediments from both the sites (C1 and W) is shown in Fig. 5.

At deeper levels of all the cores, the medium to coarse grain layers seem to suggest alternating bands of allochthonous sediment (Fig. 6). We observed abrupt changes in grain size with the bare eye, which, according to Morton et al. (2007), is one of the most reliable methods for differentiating between tsunami and storm events that involves a combination of physical characteristics and the context in which the sediment is deposited. The allochthonous/event layers observed in this study are typically characterized by variable thicknesses and poor to moderately sorted "fining upward" succession, comparable to the 2004 tsunami deposits (Fig. 5, 6, and 7). The allochthonous deposits generally lack sedimentary structures like ripple marks or small-scale cross beddings formed from bed-load transport (see Fig. 6), which are typical of storm deposits as they get deposited mainly due to the action of waves and currents associated with storms. We observed that these layers, identified as allochthonous, consist of mixed fauna rich in deep-sea foraminifera (Fig. S3), broken shells, coral debris, and rip-up plant material that shows prominent inclined stratification with alternative layers of low energy-marshy-sediments (Fig. 6). A close view of the allochthonous/event layers recovered at the different depths from all three sites are shown in Figs. 6 A-I.

Imbricated clasts and varying-sized rip-up clasts, ranging from small pebbles to large boulders, are observed in these allochthonous sediments, potentially formed by the immense force of tsunami waves that tore apart the in-situ sediment and transported it with the flow. The marks of transportation are often seen in the coarser clast from the allochthonous/event layers (Fig. 5G). The sharp bounding contacts of the allochthonous/event deposits were observed in the core sediments, which discriminated them from storm deposits (see Figs. 6 H—I).

Another distinguishing characteristic between the regular marsh sedimentation and the alternating bands of emplaced materials (referred to as 'out-of-sequence' in the beginning) is the percentage of sand present in each mode of sedimentation (Fig. 7). The remarkable congruence between the sedimentary strata of the 2004 tsunami and the allochthonous layers discovered at greater depths within the cores compel us to identify them as 'paleo-tsunami' deposits. The grain size distribution data taken at various depths from all three sites (C-1, C-2, and W) reveal a bimodal pattern in the allochthonous/event deposits, which is evident from the two distinct peaks in the plot as shown in Fig. 7. The mixed and wide range of grain sizes in allochthonous/event deposits also distinct

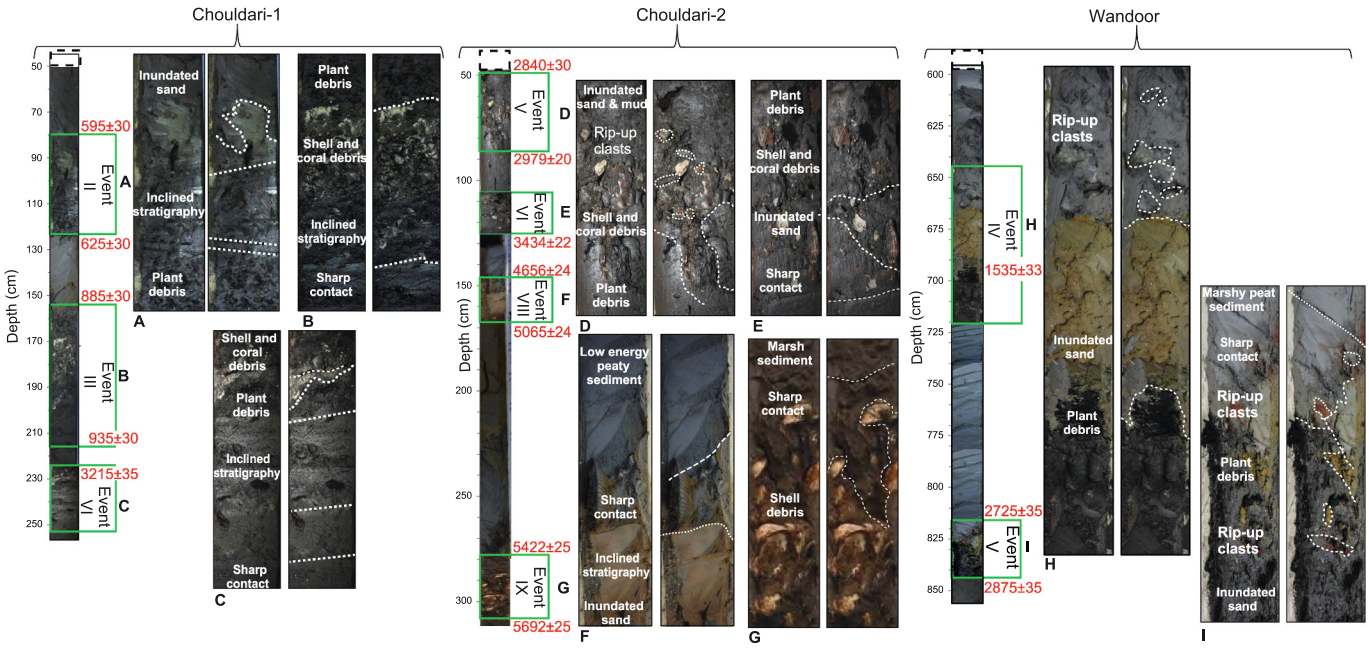

Fig. 6. Close-up views of the inundated sand (event sediment) layers recovered at the different depths from all three sites; **A-C.** The photograph shows the inundated sand layers mixed with peat, shell, and coral debris deposited by events II, III, and VI at Chouldari-1; **D-G.** The photograph shows the inundated sediment layers with peat, shell, and plant debris deposited by event V, event VI, event VIII, and event IX at Chouldari-2; H—I. Photograph showing the prominent boundary between regular marshy sediment and inundated sand layers with broken shells, coral debris, and peat deposited by the event IV and event V at Wandoor.

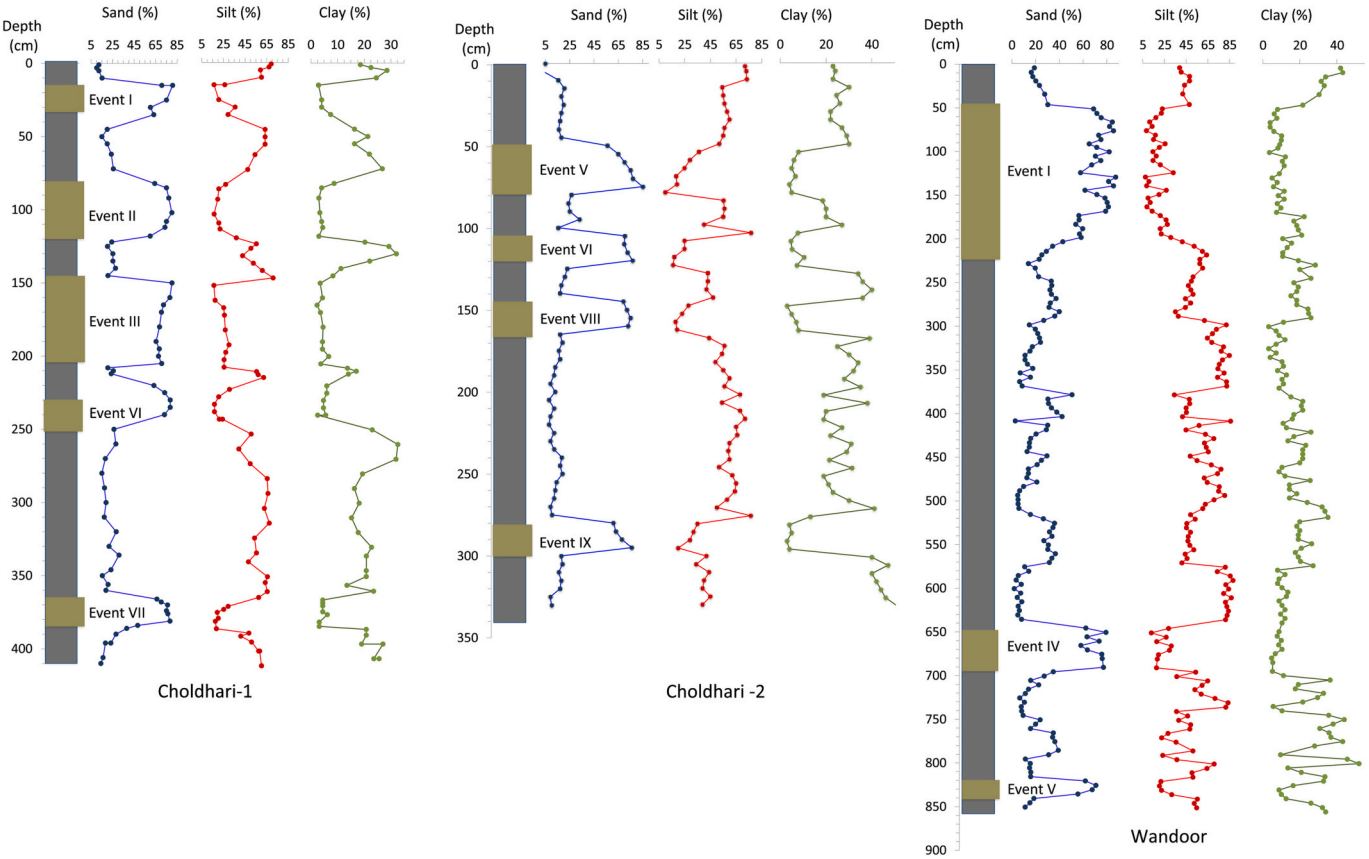

Fig. 7. Graphs representing the percentage of grain-size distributions within the core sediments analyzed at different depths from all three sites Chouldari-1, Chouldari-2, and Wandoor. The result exhibits an increasing trend of sand within the event deposits.

them from the well-sorted and narrower ranged grain sizes of storm deposits. The percentage of sand varies between 10 and 30% in the regular homogeneous marsh sediment, whereas it is ~60 to 80% in the emplaced/tsunami sediment (Fig. 7). The similar composition with high sand proportion is noted in the 2004 tsunami deposit, recovered from two sites (Chouldari-1 and Wandoor) and is also significantly richer in carbonate shells, coral, and plant debris (Figs. 5A-C and 5D-G; 8A-D). Such mixed mode typifies high-energy deposition and as mentioned earlier, is comparable to the 2004 tsunami deposits described in previous studies from the southeast coast of India and the Andaman Islands.

3.4. Microscopic analyses

The microscopic analyses were conducted on the 2004 tsunami sediments and the intermittent allochthonous deposits. The results from the site Chouldari-1indicate broken shells that comprise about 30% of the total sediment content, while organic-rich debris contributes ~45% to these deposits (Figs. 8A-D). In contrast, only a few shells (with no plant debris and coral fragments) are found in the in-situ sediment of marshy and tidal depositional settings. The dominant foraminifera in the 2004 tsunami sediments and intermittent allochthonous deposits belong to *Elphidium* sp., *Quinqueloculina* sp., and *Globigerina* sp., and are generally considered as identifiers of the marine shelf environment (Figs. 8*E*-G and Fig. S3). These faunal characteristics help in discriminating the allochthonous deposits as a mixture of transported material from the open sea from those incorporated during the landward rush of the flow. The anomalous layers are comparable to the 2004 tsunami deposits identified in the cores in terms of textural and faunal content. Thus, based on their sedimentary characteristics, micro-faunal assemblages, and transport mechanism, the coarser deposits are attributed to deposition by previous sea inundations originating as high-energy offshore tsunami events

3.5. Chronology of event layers and their far-field equivalents

Event 1 (*E*-I): The topmost levels from the cores recovered from Chouldari-1 and Wandoor contain 20-cm and 180-cm-thick sandy layers with shell, coral, and plant debris (Figs. 4A and C; 5A-E). The deposition

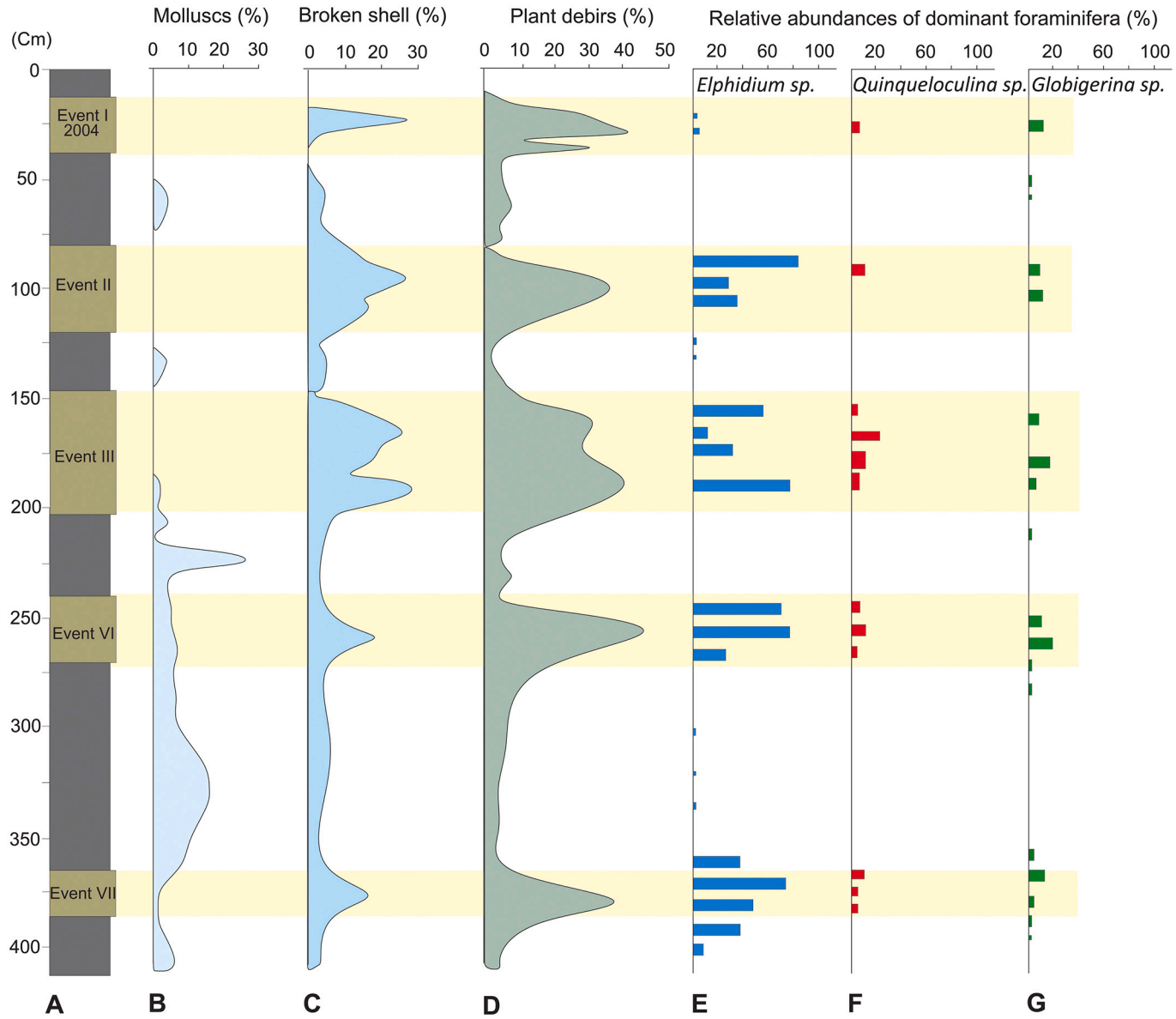

Fig. 8. A core log of Chouldari-1; **B—D.** Graphs display the representative percentage of molluscs, broken shells, and plant debris within the core sediments; **E-G.** The graph shows the relative abundance of foraminifera species in the core sediments (macro-sieve >2 mm fraction).

of this debris occurred during the 2004 tsunami, evident by some modern Carbon-14 ages marked in red (see Figs. 4A and C; Table S1). This event is chronologically compatible with the turbidite sequences generated by the 2004 event (T1), reported by Patton et al. (2015).

Event 2 (E-II): An anomalous band of coarse material was identified at a depth of 80 cm from Chouldari-1 (Figs. 4A; 6A). The organic-rich sediment samples collected from above and below this layer are dated at 590 ± 30 and 620 ± 30 yr BP, respectively (Fig. 4; Table 1, for calibrated ages of event layers). A depositional event can be placed between 596 and 606 cal. yr BP within the given margins of error. This depositional event correlates with the 14th century tsunami inundation reported from Sumatra at 620 ± 40 yr BP (ranging between 545 and 662 cal. yr BP) by Monecke et al. (2008). A comparable event is also reported from Thailand dated at 670 ± 40 yr BP (555 to 682 cal. yr BP), and 680 ± 30 yr BP (561 to 680 cal. yr BP) (Jankaew et al., 2008; Fujino et al., 2009; Fig. 9). A similar event is reported from the A&N Islands that is dated at 690 ± 23 yr BP (566 to 680 cal. yr BP), reported by Rajendran et al. (2013) (Fig. 9). This finding is also in line with the maximum limiting age of 630 ± 110 yr BP (468 to 790 cal. yr BP, termed as "event T3") as observed in the turbidite record from off Sumatra (Patton et al., 2015), providing a strong corroboration. In a more recent study, Malik et al. (2019) reported a paleotsunami event from North Andaman, and the minimum and maximum ages of this event range between 370 ± 50 and 590 ± 60, i.e., 510 and 620 cal. yr BP. Based on the historical evidence, Rajendran (2019) discusses the possibility of a contemporary tsunami in the year 1343 CE (678 yr BP) in the Indian Ocean.

Event 3 (*E*-III): Characterized by coarse to medium sand with transported coral fragments and broken shells, an anomalous deposit occurs at a depth of 147 cm at Chouldari-1 (Figs. 4A; 6B). The organic-rich sediment collected from the top and the base of this layer is dated at 880 ± 30 and 930 ± 30 yr BP (Table 1; Fig. 4A). Within the margins of error, this event occurred between 819 and 856 cal. yr BP and may correlate with the paleo-tsunami reported from A&N Islands dated at 860 ± 40 yr BP (690 and 906 cal. yr BP) and 1270 ± 30 yr BP (706 to 911 cal. yr BP) (Rajendran et al., 2008; Rajendran et al., 2013). A similar event is dated at ~950 ± 30 yr BP, ranging between 795 and 927 cal. yr BP is reported from the southeastern coast of India and from Thailand (Rajendran et al., 2006; Fujino et al., 2009; Fig. 9). This event also correlated with the tsunami event dated from the Sumatra at 960 ± 40 yr BP (786 to 952 cal. yr BP) by Monecke et al. (2008). A contemporary earthquake has been identified at 820 ± 130 yr BP ranging between 545 and 968 cal. yr BP from the turbidite sequence off Sumatra (Patton et al., 2015). An event is calculated between 726 and 984 cal. yr BP, using minimum and maximum age of 520 ± 100 and 750 ± 130 yr BP, documented from the Island of Maldives, a far-field site located in the southern Arabian Sea (Klostermann et al., 2014; Fig. 9). Similarly dated, between 802 and 1008 cal. yr BP, an inundation event on the Tanzanian coast (East Africa), is attributed to a transoceanic tsunami, also sourced in the Andaman-Sumatra region (Maselli et al., 2020; Fig. 9).

Event 4 (*E*-IV): An event layer recovered from the Wandoor site at a depth of 645 cm is dated at ~1530 ± 30 yr BP (Table 1; Figs. 4C and 6H) calibrated between 1358 and 1522 cal. yr BP. We consider this layer to have been deposited by a tsunami inundation contemporaneous with the paleo-tsunami sand sheet dated at 1400 ± 90 yr BP (1090 to 1526 cal. yr BP) near Port Blair by Rajendran et al. (2008) and from the southeast coast of India at 1581 ± 70 (1325 to 1692 cal. yr BP) by Rajendran et al. (2006); Fig. 9). This event may also coincide with an earthquake identified by Patton et al. (2015), off Sumatra with a date of 1500 ± 110 yr BP (1184 to 1689 cal. yr BP) from the turbidite sequence. A tsunami event reported by Klostermann et al. (2014) from the Maldives with a broad age range of 1030 ± 140 and 1420 ± 140 yr BP, calculated between 1485 and 1956 cal. yr BP may overlap the age interval of event 4.

Event 5 (*E*-V): Another event layer is identified in the range of 2899 and 3145 cal. yr BP at two sites: Chouldari-2 and Wandoor (Figs. 4B-C and Figs. 6D and I). The minimum ages of this event derived from organic-rich sediment of the upper boundary of the undisturbed layer at both sites (C2 and W) are 2720 ± 30 and 2870 ± 30 yr BP, respectively. The maximum age of this event is 2970 ± 20 yr BP, obtained from the lower boundary of undisturbed laminated mud (Table 1, Figs. 4B and C). These dates are comparable with the Optically Stimulated Luminescence (OSL) dates of a paleotsunami deposit in the range of 2400 to 3020 cal. yr BP, dated at 2710 ± 310 yr BP, inferred from the southern Sri Lankan coast (Premasiri et al., 2015). Jackson et al. (2014) also found an analogous event in western Sri Lanka, dated at ~2920 ± 90 yr BP (2849

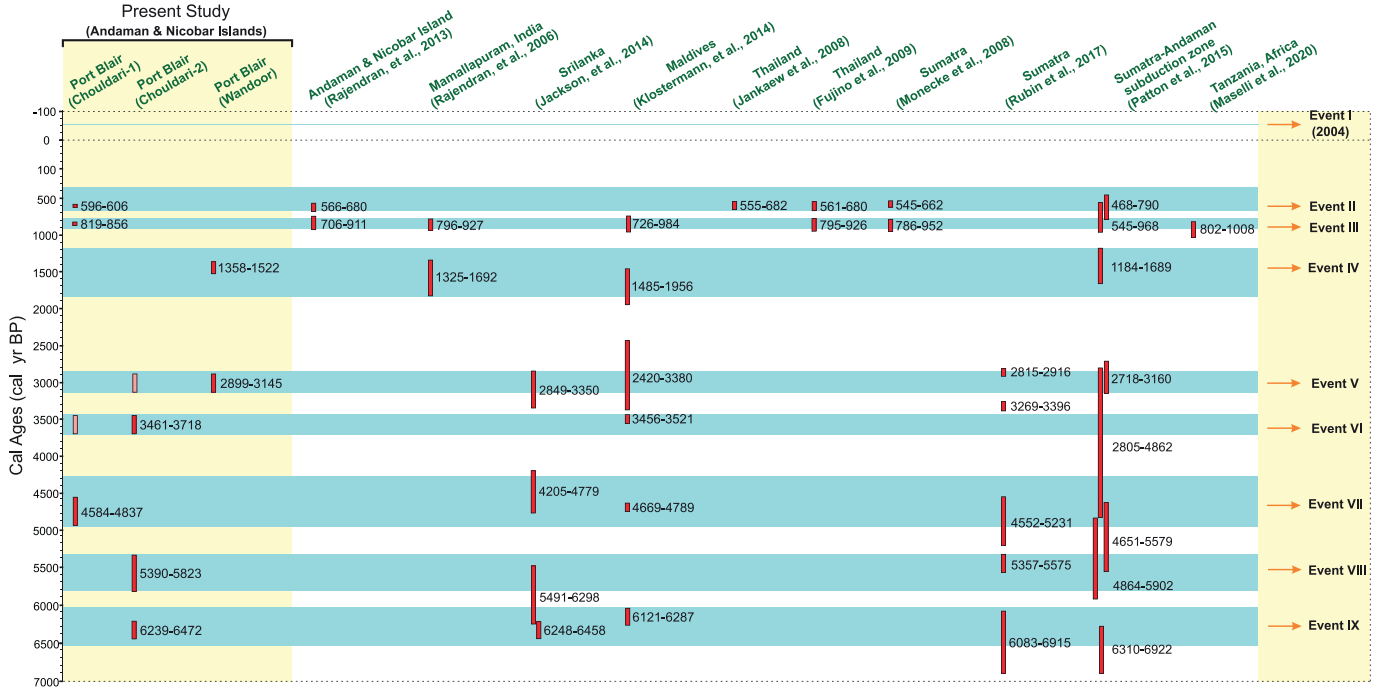

Fig. 9. Comparative space-time correlation of tsunami-event ranges from different parts of the Indian Ocean region. For each event, the age data is calibrated using Calib 7.0.2 with 2 σ range with reference to 1950, except the 2004 tsunami, which is the known event.

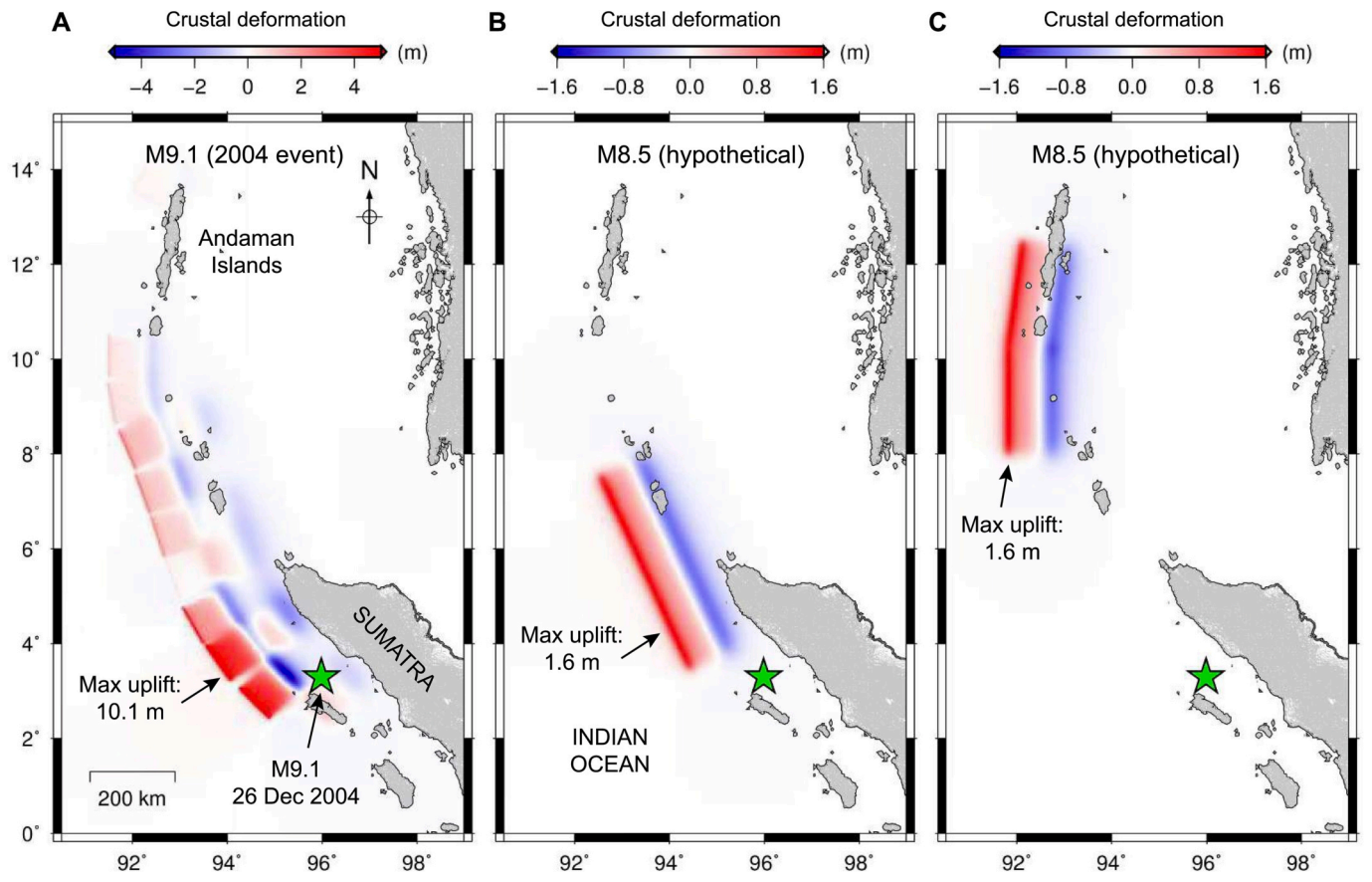

Fig. 10. Crustal deformation associated with earthquakes of differing magnitudes. **A.** The M_w 9.1 December 2004 earthquake. **B—C.** Two hypothetical M_w 8.5 events sourced from different regions of the study area. A, B, and C here correspond to tsunami modeling results shown in Figs. 2A, B, and C, respectively.

to 3350 cal. yr BP). Within the age limit, a similar event is reported by Klostermann et al. (2014), ranging between 2420 and 3380 cal. yr BP from Maldives (Fig. 9). A contemporary event is also recognized from a coastal cave in Aceh, Indonesia, with the minimum and maximum ages of 2720 ± 20 yr BP and 2820 ± 20, calculated between 2815 and 2916 cal. yr BP (Rubin et al., 2017). Two earthquake events reported by Patton et al. (2015) from the turbidite sequences off Sumatra fall within the ranges of 2718 to 3160 and 2348 to 3827 cal. yr BP (2750 ± 100 and 2920 ± 300 yr BP) (2718 to 3160 and 2348 to 3827 cal. yr BP) are also in agreement with this event, we have used the ages ranging from 2718 to 3160 yr BP event shown in Fig. 9.

Event 6 (*E*-VI): Evidence for another event was obtained from two sites at Chouldari-1 and Chouldari-2 (Figs. 4A-B; 6C and 6E) –that falls between 3461 and 3718 cal. yr BP, estimated using the maximum and minimum ages of 3430 ± 20 and 3210 ± 30 yr BP of the organic-rich sediment at the lower and top contact zones of the event layer (Table 1; Figs. 4A-B). This may correspond to an event dated from the Maldives between 3210 ± 30 and 3280 ± 30 cal. yr BP, which is calculated with a range of 3456 to 3521 cal. yr BP (Klostermann et al., 2014; Fig. 9). Similar timing for a previous tsunami is obtained from the southern coast of Sri Lanka with the OSL age of 3170 ± 320 yr BP (2850 to 3490 cal. yr BP) (Premasiri et al., 2015). The maximum age of the tsunami sand sheet recognized from a coastal cave in Aceh, Indonesia, deposited between 3269 and 3396 cal. yr BP (Rubin et al., 2017), and might thus represent a contemporaneous transoceanic event (Fig. 9). Within the age limit, this event also corresponds well with an earthquake event dated at 3530 ± 400 (2805 to 4862 cal. yr BP) by Patton et al. (2015) (Fig. 9).

Event 7 (E-VII): Identified at the Chouldari-1 site, the depositional age of event 7 at a depth of 365 cm is constrained based on organic-rich sediment age of 4180 ± 30 yr BP, obtained from the organic debris within the inundated sediment (Table 1; Fig. 4A). Ranging between 4584 and 4837 cal. yr BP, this event may correspond with an earlier tsunami event in the Maldives, dated between 4110 ± 30 and 4210 ± 30 cal. yr BP (calculated between 4669 and 4789 cal. yr BP) by Klostermann et al. (2014) (Fig. 9). This event also corresponds with an event calculated between 4205 and 4779 cal. yr BP by using the minimum and maximum age of the event from western Sri Lanka (Jackson et al., 2014). Similarly, Rubin et al. (2017) tag an event in the range of 4552 and 5231 cal. yr BP (Fig. 9). And, within the chronological uncertainty, this event may coincide with the event dated at 4460 ± 150 yr BP ranging between 4651 and 5579 cal. yr BP, off Sumatra, recognized from the turbidite sequence (Patton et al., 2015; Fig. 9).

Event 8 (E-VIII): The minimum and maximum ages (4650 ± 20–5060 ± 20 yr BP) of the organic-rich sediment obtained from the undisturbed organic mud above and below the 20-cm-thick event deposit from Chouldari-2 site constrain the depositional age of event 8 between 5390 and 5823 cal. yr BP. This layer is characterized by coarse sand with shell debris at a depth of 145 cm (Table 1; Figs. 4B; 6F). This event also corresponds with an event calculated between 5491 and 6298 cal. yr BP by using the minimum and maximum age of the event documented from western Sri Lanka (Jackson et al., 2014). A similar event, dated at 4660 ± 40 yr BP by Rubin et al. (2017) from Indonesia falls in the similar range between 5357 and 5575 cal. yr BP. Indication of a contemporaneous earthquake dated at 4720 ± 220 yr BP (4864 and 5902 cal. yr BP; Fig. 9) is obtained from the turbidite sequence located off Sumatra (Patton et al., 2015; Fig. 9).

Event 9 (*E*-IX): The oldest tsunami in this sequence is identified from the Chouldari-2 site (Fig. 4B and Fig. 6G). The bottom and top of the event layer are dated at 5690 ± 20 yr BP and 5420 ± 20 yr BP, respectively (Fig. 4B). Using these constraints, the timing of event 9 is approximated between 6239 and 6472 cal. yr BP (Table 1) may

correspond with an event dated at 5400 ± 30 yr BP in the range of 6121 and 6287 cal. yr BP, documented from Maldives (Klostermann et al., 2014) (Fig. 9). An event layer whose ages are dated at 5410 ± 50 yr BP and 5450 ± 35 yr BP, calculated between 6248 and 6458 cal. yr BP, as reported from the Karagan Lagoon, Sri Lanka (Jackson et al., 2014), may belong to this regional tsunami (Fig. 9). A sea transgression of the same period dated at 6060 ± 40 yr BP (6083–6915 cal. yr BP) has also been obtained from the cave deposits from the Sumatran Coast (Rubin et al., 2017; Fig. 9). Evidence for earthquakes at 5790 ± 140 (6301 to 6922 cal. yr BP), recorded from Sumatra by Patton et al. (2015). A possible contemporary event ranging between 6500 and 7000 cal. yr BP is recorded in Aceh, Indonesia by Pre et al. (2012).

4. Discussion

We have identified nine event layers in the cores collected from South Andaman, including the 2004 tsunami, within a timescale of about 6000 years. The timeline developed for the tsunami events in this study, and the comparable intervals obtained from the distant sites in the Indian Ocean (with margins of error) implies that all those depositions are products of temporally correlative transoceanic tsunamis. In this context, one factor worth mentioning is the respective sensitivities of the various types of records discussed and how that plays into such comparisons. The turbidite record off Sumatra (Patton et al., 2015), for example, reveals ~10 events in the quiescent period proposed in this study, but this may be entirely expected from the higher sensitivity to ground motions (~ Mw 6–7) than a tsunami record, reflecting the events of magnitude $M_w \geq 8.0$, assuming that all the turbidite sequences are representative of earthquakes.

As discussed earlier, the tsunami simulations helped in benchmarking the propagation patterns of hypothetical events of lesser magnitudes, as compared to the 2004 M_w 9.1 event, and their possible extent of impacts on the near and distant coasts. It has become clear that the location variations in the sources of these modeled tsunamigenic earthquakes determine their directivities and, therefore, their impacts on near−/far-field locations in the Indian Ocean region. The transoceanic reach of the two hypothetical tsunamis simulated in this study shows that the events can variously affect some of the regions bordering the Indian Ocean — a determining factor for their directivity being the location of their source areas. However, in terms of spatial coverage, only a 2004-type event could reach all near-field and far-field locations included in this study. Although we benchmark the past events discussed here as greater than magnitude 8.5 and tending towards 9, our study does not attempt to quantify their magnitudes.

The age uncertainties and the possibility of the incompleteness of historic and paleoseismic data add to the challenge of precisely

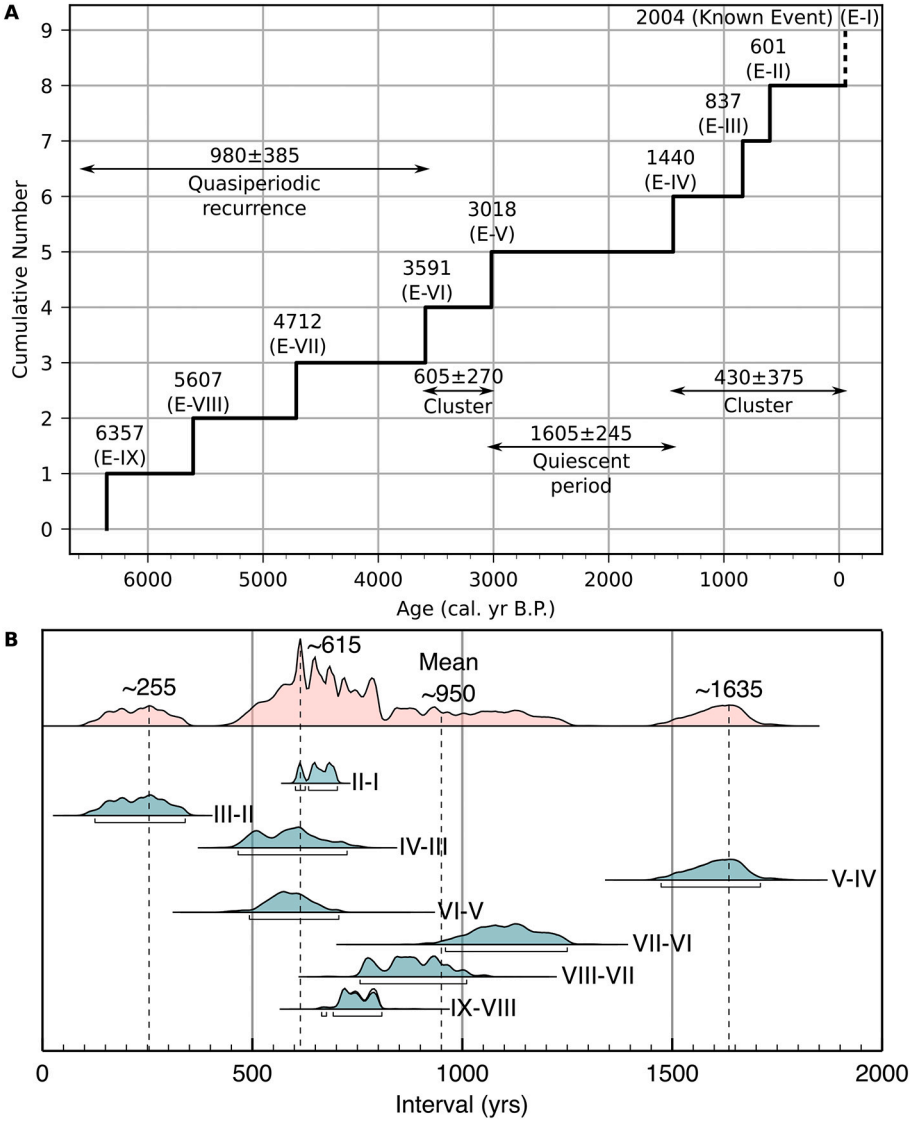

Fig. 11. A. The temporal pattern of the nine events from this study, with their cumulative number (y-axis) plotted against their age in cal. yr BP. The midpoint ages correspond to Table 1. The temporal pattern follows a Devil's Staircase-like trend (Chen et al., 2020). **B.** The modeled recurrence pattern of tsunami deposits from this study. The inter-event periods (interval between events II-I, III-II, and so on) are shown as blue curves, with the most recent period at the top (II-I, between the 2004 and ~ 601 cal. yr BP events). The overall pattern of recurrence is shown in pink at the top. The recurrence pattern has a mode of ~615 years and a mean of ~950 years. The inter-event periods III-II and V-IV do not overlap with the remaining periods and mark the extent of variability in the recurrence interval. The intervals in both (a) and (b) were obtained using the Difference() function in OxCal (Bronk Ramsey, 2008). (For interpretation of the references to colour in this figure legend, the reader is referred to the web version of this article.)

identifying complex temporal patterns in earthquake recurrence (Kempf et al., 2019; Chen et al., 2020). Further, rigorous statistical analysis requires either instrumental or historical earthquake records (Chen et al., 2020), or a combination of both, with enough events to obtain a representative recurrence interval (Pizer et al., 2021). The inferences presented in this study should be viewed in the context of such constraints, as the stratigraphic uncertainty (in terms of preservation) increases as we go further into the past. The preservation of event layers improves towards the more recent geological past (the last ~2000 yr BP), where we could observe the clustering of events after a relatively longer quiescent interval(s).

As shown in Fig. 11A, we observe quasiperiodic recurrence (980 ± 385 years) for events *E*-VI to E-IX from 3590 cal. yr BP (3461–3718 cal. yr BP) to 6357 cal. yr BP (6239–6472 cal. yr BP).After an interval of quiescence that lasted 1605 ± 245 years following the 3018 cal. yr BP event (E-V, 2899–3145 cal. yr BP), the events E-I to E-IV took place in relatively close succession over ~1494 yr (interval of 430 ± 375 years), especially the E-II at 601 cal. yr BP (596–606 cal. yr BP) and E-III at ~837 cal. yr BP (819–856 cal. yr BP), with a long hiatus of 220 ± 185 years between them. An interval extending to 605 ± 270 years is recorded between E-V and E-VI, which is much shorter than the preceding and succeeding intervals, and hence, we loosely characterize E-V and E-VI as a temporal cluster. Such a combination of quasiperiodic (E-VI to E-IX) and 'burstier' sequence (E-I to E-IV, and to some extent, E-V and E-VI) has also been observed elsewhere.

For the nine events identified in the present study, the corresponding eight inter-event periods range from 220 ± 185 to 1605 ± 245 years. The modeled recurrence pattern of the events discussed in this study is shown in Fig. 11B. We observe a mode at ~615 years and a mean of ~950 years. The two inter-event periods, III-II (220 ± 185 years) and V-IV (1605 ± 245 years), highlight the variability in event recurrence.

Ratzov et al. (2015) observed similar time scales over the past ~8000 years at the Africa-Eurasia plate boundary off west Algeria. They identified 13 paleo-earthquakes distributed across three ~300–600-yr-long clusters, separated by quiescent periods of ~1600 yr. Termed as 'supercycles', such temporal variability in earthquake recurrence intervals has also been suggested for the southern part of the Sunda megathrust (Sieh et al., 2008; Rubin et al., 2017) and the Cascadia margin in the northwest United States (Goldfinger et al., 2012). Rather than representative of a temporal behavior, these results indicating variable recurrence regimes of mega earthquakes-cum-tsunamis presented here should be considered as reflective of variable strain accumulation and release over a series of partial and full ruptures – a conclusion that can be drawn from of super cycle models of Sieh et al. (2008), Goldfinger et al. (2013), Satake (2015), and the Long-Term Fault Memory model of Salditch et al. (2020).

The tsunami chronology developed here for the Indian Ocean suggests temporally variable phases of recurrence regimes for great tsunami earthquakes. The database suggests an earlier phase of quasiperiodic earthquake recurrences and a later 'burstier' sequence with event cluster (s) separated by irregular, long interval(s) of quiescence. Such a pattern, mathematically described as 'Devil's Staircase' by Chen et al. (2020), can be attributed to the pattern of tsunami-earthquake recurrence discussed in this study (Fig. 11A). The pattern of great/mega earthquakes with quasiperiodic intervals is supported by the elastic rebound model, as introduced by Reid (1910). However, the assumptions of constant loading rates and cyclic strain accumulation and release need not always hold (Chen et al., 2020), as evidenced by complex temporal patterns of earthquake recurrence observed in longer records. These complex temporal patterns consisting of quiescent intervals between clusters are also identified in the present study. The duration of the quiescent periods could be inversely related to the tectonic loading (or slip) rates (Satake and Atwater, 2007; Chen et al., 2020). The clusters themselves are possibly a function of the fault interaction and viscoelastic relaxation (Chen et al., 2020). They have been modeled to originate from random variations of the fault yield stress between earthquakes (DiCaprio et al., 2008).

5. Conclusions

For the nine events identified in the present study, the corresponding eight inter-event periods range from 220 ± 185 to 1605 ± 245 years. The modeled recurrence pattern of the events discussed in this study is shown in Fig. 11B. We observe a mode at ~615 years and a mean of ~950 years. The two inter-event periods, III-II (220 ± 185 years) and V-IV (1605 ± 245 years), highlight the variability in event recurrence. The long-term recurrence characteristics of the 2004-type earthquakes along the Sumatra-Andaman subduction zone presented in this study provide an independent baseline data for testing the assumptions on such theoretical models and simulations where the variability of accumulated strain within the fault zone determines the probability of the next large earthquake, rather than the elapsed time. Our findings have implications for re-estimating the probabilities of mega earthquakes along the subduction zones. A fundamental question about hazard estimation in the Andaman-Sumatra region is whether the last sequence of events to have occurred, ending with the 2004 earthquake, is part of an ongoing cluster or it marks the end of that cycle. These distinct opposing scenarios may lead to variable estimates of earthquake probabilities.

Declaration of Competing Interest

We have no conflicts of interest to disclose.

Data availability

The authors declare that all data supporting the findings of this study are available within the article, its supplementary information, and available at Earth and Space Science Open Archive [ESSOAr] via [doi.org/10.1002/essoar.10504555.1].

Acknowledgments

This study was funded by the Indian National Centre for Ocean Information Services, Hyderabad, India (INCOIS: F&A:XII:B1:018, 2013) and the Board of Research in Nuclear Sciences, Department of Atomic Energy, Government of India (36(2)/14/48/2016-BRNS/36121.2017) to C.P.R. Radiocarbon dating of the samples was conducted at Poznan Radiocarbon Laboratory, Poland. We thank Prof. Marc De Batist (Ghent University, Belgium) for reviewing an earlier version of the manuscript. We greatly value the critical evaluation by three anonymous referees, and sincerely appreciate the comments and suggestions.

Appendix A. Supplementary data

Supplementary data to this article can be found online at https://doi.org/10.1016/j.margeo.2023.107051.

References

Ammon, C.J., Ji, C., Thio, H., Robinson, D., Ni, S., Hjorleifsdottir, V., Kanamori, H., Thorne, L., Das, S., Helmberger, D., Ichlinose, G., Polet, J., Wald, D., 2005. Rupture process of the 2004 Sumatra-Andaman Earthquake. Science 308, 1133–1139.

Andrade, V., Rajendran, K., Rajendran, C.P., 2014. Sheltered coastal environments as archives of paleo-tsunami deposits: Observations from the 2004 Indian Ocean tsunami. J. Asian Earth Sci. 95, 331–341.

Blaauw, M., Christen, J.A., 2011. Flexible paleoclimate age-depth models using an autoregressive gamma process. Bayesian Anal. 6 (3), 457–474. https://doi.org/10.1214/11-BA618.

Chen, Y., Liu, M., Luo, G., 2020. Complex temporal patterns of large earthquakes: Devil's staircases. Bull. Seismol. Soc. Am. 110, 1064–1076. https://doi.org/10.1785/0120190148.

Cordova, J., 2014. Analysis of a Potential Paleotsunami Deposit at Los Penasquitos Marsh. San Diego County, CA.

Costa, P.J., Dawson, S., Ramalho, R.S., Engel, M., Dourado, F., Bosnic, I., Andrade, C., 2021. A review on onshore tsunami deposits along the Atlantic coasts. Earth Sci. Rev. 212, 103441 https://doi.org/10.1016/j.earscirev.2020.103441.

Dawson, A.G., 1994. Geomorphological effects of tsunami run-up and backwash. In Geomorph and nat haz. 83–94.
Dharanirajan, K., Kasinatha Pandian, P., Gurugnanam, B., Narayanan, R., Ramachandran, S., 2007. An integrated study for the assessment of tsunami impacts: a case study of south Andaman Island, India using remote sensing and GIS. Coast. Eng. J. 49 (3), 229–266. https://doi.org/10.1142/S0578563407001617.
DiCaprio, C.J., Simons, M., Kenner, S.J., Williams, C.A., 2008. Post-seismic reloading and temporal clustering on a single fault. Geophys. J. Int. 172 https://doi.org/10.1111/j.1365-246X.2007. 03622.x, 581-214 592.
Folk, R.L., Ward, W.C., 1957. Brazos river bar [Texas]; a study in the significance of grain size parameters. J. Sediment. Res. 27, 3–26.
Fujii, Y., Satake, K., 2007. Tsunami source of the 2004 Sumatra–Andaman earthquake inferred from tide gauge and satellite data. Bull. Seismol. Soc. Am. 97 (1A), S192–S207.
Fujino, S., Naruse, H., Matsumoto, D., Jarupongsakul, T., Sphawajruksakul, A., Sakakura, N., 2009. Stratigraphic evidence for pre-2004 tsunamis in southwestern Thailand. Mar. Geol. 262, 25–28.
Gelfenbaum, G., Vatvani, D., Jaffe, B., Dekker, F., 2007. Tsunami inundation and sediment transport in vicinity of coastal mangrove forest. In Coast Sediment 7, 1117–1128.
Goff, J., Chagué-Goff, C., Nichol, S., 2001. Palaeotsunami deposits: a New Zealand perspective. Sedi. Geol. 143 (1–2), 1–6.
Goff, J., Chagué-Goff, C., Nichol, S., Jaffe, B., Dominey-Howes, D., 2012. Progress in palaeotsunami research. Sediment. Geol. 243, 70–88.
Goldfinger, C., Nelson, C.H., Morey, A.E., Johnson, J.E., Patton, J.R., Karabanov, E.B., Gutierrez-Pastor, J., Eriksson, A.T., Gracia, E., Dunhill, G., Enkin, R.J., 2012. Turbidite Event History-Methods and Implications for Holocene Paleoseismicity of the Cascadia Subduction Zone (No. 1661-F). US Geological Survey.
Goldfinger, C., Ikeda, Y., Yeats, R.S., Ren, J., 2013. Super quakes and super cycles. Seismol. Res. Lett. 84 (1), 24–32.
Griffin, J.D., Stirling, M.W., Wang, T., 2020. Periodicity and clustering in the long-term earthquake record. Geophys. Res. Lett. 47 https://doi.org/10.1029/2020GL089272 e2020GL089272.
Heidarzadeh, M., Ishibe, T., Sandanbata, O., Muhari, A., Wijanarto, A.B., 2020. Numerical modeling of the subaerial landslide source of the 22 December 2018 Anak Krakatoa volcanic tsunami, Indonesia. Ocean Eng. 195 https://doi.org/10.1016/j.oceaneng.2019.106733.
Heidarzadeh, M., Gusman, A., Ishibe, T., Sabeti, R., Šepić, J., 2022. Estimating the eruption-induced water displacement source of the 15 January 2022 Tonga volcanic tsunami from tsunami spectra and numerical modelling. Ocean Eng. 261, 112165 https://doi.org/10.1016/j.oceaneng.2022.112165.
Hori, K., Kuzumoto, R., Hirouchi, D., Umitsu, M., Janjirawuttikul, N., Patanakanog, B., 2007. Horizontal and vertical variation of 2004 Indian tsunami deposits: an example of two transects along the western coast of Thailand. Mar. Geol. 239 (3–4), 163–172.
India Meteorological Department, 2008. Tracks of Cyclones and Depressions in the Bay of Bengal and Arabian Sea, pp. 1891–2007.
Jackson, K.L., Eberli, G.P., Amelung, F., McFadden, M.A., Moore, A.L., Rankey, E.C., Jayasena, H., 2014. Holocene Indian Ocean tsunami history in Sri Lanka. Geology 42, 859–862.
Jaffe, B.E., Morton, R.A., Kortekaas, S., Dawson, A.G., Smith, D.E., Gelfenbaum, G., Foster, I.D., Long, D., Shi, S., 2008. Reply to Bridge (2008) discussion of articles in 'sedimentary features of tsunami deposits. Sedi. Geol. 211 (3–4), 95–97.
Jankaew, K., Atwater, B.F., Sawai, Y., Choowong, M., Charoentitirat, T., Martin, M.E., Prendergast, A., 2008. Medieval forewarning of the 2004 Indian Ocean tsunami in Thailand. Nature 455, 1228–1231.
Kempf, P., Moernaut, J., Batist, M.D., 2019. Bimodal recurrence pattern of tsunamis in south-Central Chile: a statistical exploration of paleotsunami data. Seismol. Res. Lett. 90 (1), 194–202.
Klostermann, L., Gischler, E., Storz, D., Hudson, J.H., 2014. Sedimentary record of late Holocene event beds in a mid-ocean at Oll Lagoon, Maldives, Indian Ocean: potential for deposition by tsunamis. Mar. Geol. 348, 37–43.
Liu, P.L.F., Woo, S.B., Cho, Y.S., 1998. Computer Programs for Tsunami Propagation and Inundation. Technical Report. Cornell University, Ithaca, New York.
Malik, J.N., Shishikura, M., Echigo, T., Ikeda, Y., Satake, K., Kayanne, H., Sawai, Y., Murty, C.V.R., Dikshit, O., 2011. Geological evidence for two pre-2004 earthquakes during recent centuries near Port Blair, South Andaman Island, India. Geology 39, 559–562.
Malik, J.N., Johnson, F.C., Khan, A., Sahoo, S., Irshad, R., Paul, D., Arora, S., Baghel, P. K., Chopra, S., 2019. Tsunami records of the last 8000 years in the Andaman Island, India, from mega and large earthquakes: Insights on recurrence interval. Sci. Rep. 9, 1–14.
Maselli, V., Oppo, D., Moore, A.L., Gusman, A.R., Mtelela, C., Iacopini, D., Taviani, M., Mjema, E., Mulaya, E., Che, M., Tomioka, A.L., 2020. A 1000-yr-old tsunami in the Indian Ocean points to greater risk for East Africa. Geology 48 (8), 808–813.
Meltzner, A.J., Sieh, K., Chiang, H.W., Shen, C.C., Suwargadi, B.W., Natawidjaja, D.H., Philibosian, B.E., Briggs, R.W., Galetzka, J., 2010. Coral evidence for earthquake recurrence and an ad 1390–1455 cluster at the south end of the 2004 Aceh–Andaman rupture. J. Geophys. Res. Solid Earth 115 (B10).
Monecke, K., Finger, W., Klarer, D., Kongko, W., McAdoo, B.G., Moore, A.L., Sudrajat, S. U., 2008. A 1,000-year sediment record of tsunami recurrence in northern Sumatra. Nature 455, 1232–1234.
Moore, A.L., McAdoo, B.G., Ruffman, A., 2007. Landward fining from multiple sources in a sand sheet deposited by the 1929 Grand Banks tsunami, Newfoundland. Sediment. Geol. 200 (3–4), 336–346.
Morton, R.A., Gelfenbaum, G., Jaffe, B.E., 2007. Physical criteria for distinguishing sandy tsunami and storm deposits using modern examples. Sediment. Geol. 200 (3–4), 184–207.
Nagendra, R., Kamala Kannan, B.V., Sajith, C., Sen, Gargi, Reddy, A.N., Srinivasalu, S., 2005. A record of foraminiferal assemblage in tsunami sediments along Nagappattinam Coast, Tamil Nadu. Curr. Sci. 89, 1947–1952.
Okada, Y., 1985. Surface deformation due to shear and tensile faults in a half-space. Bull. Seismol. Soc. Am. 75 (4), 1135–1154.
Patton, J.R., Goldfinger, C., Morey, A.E., Ikehara, K., Romsos, C., Stoner, J., Djadjadihardja, Y., Ardhyastuti, S., Gaffar, E.Z., Vizcaino, A., 2015. A 6600-year earthquake history in the region of the 2004 Sumatra-Andaman subduction zone earthquake. Geosphere 11, 2067–2129.
Philibosian, B., Meltzner, A.J., 2020. Segmentation and super cycles: a catalog of earthquake rupture patterns from the Sumatran Sunda Megathrust and other well-studied faults worldwide. Quat. Sci. Rev. 241, 106390.
Pizer, C., Clark, K., Howarth, J., Garrett, E., Wang, X., Rhoades, D., Woodroffe, S., 2021. Paleotsunamis on the Southern Hikurangi Subduction Zone, New Zealand, show regular recurrence of large subduction earthquakes. The Seismic Record 1 (2), 75–84.
Pre, C.A.G., Horton, B.P., Kelsey, H.M., Rubin, C.M., Hawkes, A.D., Dary-ono, M.R., Rosenberg, G., Culver, S.J., 2012. Stratigraphic evidence for an early Holocene earthquake in Aceh, Indonesia. Quat. Sci. Rev. 54, 142–151.
Premasiri, R., Styles, P., Shrira, V., Cassidy, N., Schwenninger, J.L., 2015. OSL dating and GPR mapping of palaeotsunami inundation: a 4000-year history of Indian Ocean tsunamis as recorded in Sri Lanka. Pure Appl. Geophys. 172, 3357–3384.
Rajendran, K., 2013. On the recurrence of great subduction zone earthquakes. Curr. Sci. 104, 880–892.
Rajendran, C.P., 2019. Historical accounts of sea disturbances from South India and their bearing on the penultimate predecessor of the 2004 tsunami. Seismol. Res. Lett. 90, 774–783.
Rajendran, C.P., Rajendran, K., Machado, T., Satyamurthy, T., Aravazhi, P., Jaiswal, M., 2006. Evidence of ancient sea surges at the Mamallapuram Coast of India and implications for previous Indian Ocean tsunami events. Curr. Sci. 91, 1242–1247.
Rajendran, C.P., Rajendran, K., Anu, R., Earnest, A., Machado, T., Mohan, P.M., Freymueller, J., 2007. Crustal deformation and seismic history associated with the 2004 Indian Ocean earthquake: a perspective from the Andaman–Nicobar Islands. Bull. Seismol. Soc. Am. 97 (1A), S174–S191.
Rajendran, K., Rajendran, C.P., Earnest, A., Prasad, G.R., Dutta, K., Ray, D., Anu, R., 2008. Age estimates of coastal terraces in the Andaman and Nicobar Islands and their tectonic implications. Tectonophysics 455, 53–60.
Rajendran, C.P., Rajendran, K., Srinivasalu, S., Andrade, V., Aravazhi, P., Sanwal, J., 2011. Geoarchaeological evidence of a Chola-period tsunami from an ancient port at Kaveripattinam on the Southeastern Coast of India. Geoarchaeology 26, 867–887.
Rajendran, C.P., Rajendran, K., Andrade, V., Srinivasalu, S., 2013. Ages and relative sizes of pre-2004 tsunamis in the Bay of Bengal inferred from geologic evidence in the Andaman and Nicobar Islands. J. Geophys. Res. Solid Earth 118, 1345–1362.
Ramsey, C.B., 2008. Deposition models for chronological records. Quat. Sci. Rev. 27 (1–2), 42–60.
Ratzov, G., Cattaneo, A., Babonneau, N., Déverchère, J., Yelles, K., Bracene, R., Courboulex, F., 2015. Holocene turbidites record earthquake supercycles at a slow-rate plate boundary. Geology 43 (4), 331–334.
Reid, H.F., 1910. The Mechanics of the Earthquake, in the California Earthquake of April 18, 1906: Report of the State Earthquake Investigation Commission, vol. v. 87. Carnegie Institution of Washington Publication, p. 192 (reprinted in 1969).
Reimer, P.J., Bard, E., Bayliss, A., Beck, J.W., Blackwell, P.G., Ramsey, C.B., Buck, C.E., Cheng, H., Edwards, R.L., Friedrich, M., Grootes, P.M., 2013. Intcal13 and marine13 radiocarbon age calibration curves 0–50,000 years cal BP. Radiocarbon 55, 1869–1887.
Rubin, C.M., Horton, B.P., Sieh, K., Pilarczyk, J.E., Daly, P., Ismail, N., Parnell, A.C., 2017. Highly variable recurrence of tsunamis in the 7,400 years before the 2004 Indian Ocean tsunami. Nat. Commun. 8 (1), 1–12.
Salditch, L., Stein, S., Neely, J., Spencer, B.D., Brooks, E.M., Agnon, A., Liu, M., 2020. Earthquake supercycles and long-term fault memory. Tectonophysics 774, 228–289.
Satake, K., 2015. Geological and historical evidence of irregular recurrent earthquakes in Japan. Philos. Trans. R. Soc. A Math. Phys. Eng. Sci. 373 (2053), 20140375.
Satake, K., Atwater, B.F., 2007. Long-term perspectives on giant earthquakes and tsunamis at subduction zones. Annu. Rev. Earth Planet. Sci. 35, 349–374.
Satake, K., Heidarzadeh, M., Quiroz, M., Cienfuegos, R., 2020. History and features of trans-oceanic tsunamis and implications for paleo-tsunami studies. Earth Sci. Rev. 202, 103112.
Satish Kumar, V., Babu, V.R., Babu, M.T., Dhinakaran, G., Rajamanickam, G.V., 2008. Assessment of storm surge disaster potential for the Andaman Islands. J. Coast. Res. 24 (10024), 171–177.
Sawai, Y., Namegaya, Y., Okamura, Y., Satake, K., Shishikura, M., 2012. Challenges of anticipating the 2011 Tohoku earthquake and tsunami using coastal geology. Geophys. Res. Lett. 39 (21), 1–6.
Sieh, K., Natawidjaja, D.H., Meltzner, A.J., Shen, C.C., Cheng, H., Li, K.S., Suwargadi, B. W., Galetzka, J., Philibosian, B., Edwards, R.L., 2008. Earthquake supercycles inferred from sea-level changes recorded in the corals of West Sumatra. Science 322, 1674–1678.
Srinivasalu, S., Rajeshwara Rao, N., Thangadurai, N., Jonathan, M.P., Roy, P.D., Ram Mohan, V., Saravanan, P., 2009. Characteristics of 2004 tsunami deposits of the northern Tamil Nadu coast, southeastern India. Boletin de la Soc. Geol. Mex. 61 (1), 111–118.

Srinivasalu, S., Thangadurai, N., Switzer, A.D., Ram Mohan, V., Ayyamperumal, T., 2007. Erosion and sedimentation in Kalpakkam (N Tamil Nadu, India) from the 26th December 2004 tsunami. Mar. Geol. 240, 65–75.
Stuiver, M., Reimer, P.J., 1993. Extended 14C data base and revised CALIB 3.0 14C age calibration program. Radiocarbon 35 (1), 215–230.
Varikkodan, H., Balaji, S., Arjun, S., Mandal, K.K., 2023. Tropical cyclone risk assessment of Port Blair, Andaman Islands, India by using numerical modelling and geospatial techniques. J. Earth System Sci. 132 (1), 37.
Wang, X., Liu, P.L.F., 2006. An analysis of 2004 Sumatra earthquake fault plane mechanisms and Indian Ocean tsunami. J. Hydraul. Res. 44, 147–154.
Weatherall, P., Marks, K.M., Jakobsson, M., Schmitt, T., Tani, S., Arndt, J.E., Rovere, M., Chaye, D., Ferrini, V., Wigley, R., 2015. A new digital bathymetric model of the world's oceans. Earth Space Sci. 2, 331–345.